AD-A127 430 SEISMIC DISCRIMINATION AT REGIONAL DISTANCE(U) NEVADA 1/1
UNIV RENO SEISMOLOGICAL LAB K F PRIESTLEY ET AL.
21 MAR 83 AFOSR-TR-83-0276 AFOSR-81-0006

UNCLASSIFIED F/G 8/11 NL

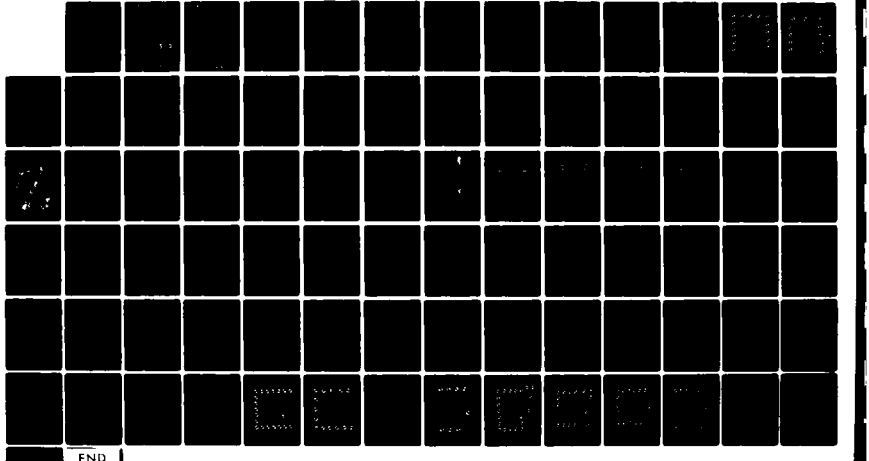

END
DATE FILMED
6-83
DTIC

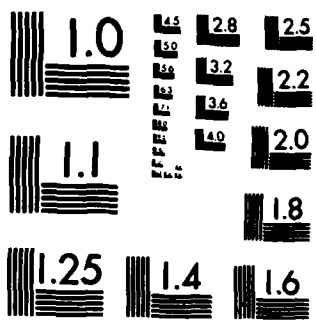

UNCLASSIFIED

(5)

SECURITY CLASSIFICATION OF THIS PAGE (When Data Entered)

REPORT DOCUMENTATION PAGE	READ INSTRUCTIONS BEFORE COMPLETING FORM
1. REPORT NUMBER: AFOSR-TR- 83-0276	2. GOVT ACCESSION NO.: A127430
3. RECIPIENT'S CATALOG NUMBER	
4. TITLE (and Subtitle): SEISMIC DISCRIMINATION AT REGIONAL DISTANCE	5. TYPE OF REPORT & PERIOD COVERED: Final 1/10/81 - 31/9/82
	6. PERFORMING ORG. REPORT NUMBER
7. AUTHOR(s): Keith F. Priestley Alan S. Ryall	8. CONTRACT OR GRANT NUMBER(s): AFOSR-81-0006
9. PERFORMING ORGANIZATION NAME AND ADDRESS: Seismological Laboratory University of Nevada Reno, Nv 89557-0018	10. PROGRAM ELEMENT, PROJECT, TASK AREA & WORK UNIT NUMBERS: 61101E 2309/A1
11. CONTROLLING OFFICE NAME AND ADDRESS: Defense Advanced Research Projects Agency 1400 Wilson Blvd Arlington, Va 22209	12. REPORT DATE: 21 March 1983 13. NUMBER OF PAGES: 73
14. MONITORING AGENCY NAME & ADDRESS (if different from Controlling Office): Air Force Office of Scientific Research Bolling AFB/Bldg 410 Washington, D.C. 20332	15. SECURITY CLASS. (of this report): Unclassified 15a. DECLASSIFICATION/DOWNGRADING SCHEDULE

16. DISTRIBUTION STATEMENT (of this Report)

Unlimited

Approved for public release; distribution unlimited.

17. DISTRIBUTION STATEMENT (of the abstract entered in Block 20, if different from Report)

Unlimited

DTIC ELECTE S APR 29 1983 D E

18. SUPPLEMENTARY NOTES

19. KEY WORDS (Continue on reverse side if necessary and identify by block number)

Stress variation, Tectonic release, Faultless, m_b, P-wave residuals

20. ABSTRACT (Continue on reverse side if necessary and identify by block number)

The research supported by this grant is directed towards the general problems of discrimination and yield estimation. During the past year has evolved along two lines: 1) analysis of stress variation within the crust and its possible effects on "tectonic release"; and 2) effects of large scale mantle structure and crustal focusing/defocusing on parameters such as m_b, trace amplitude, period and t^* over short distances near the *Faultless* shot point.

DD FORM 1 JAN 73 1473

UNCLASSIFIED

In section I and appendix A, the effects of stress distribution within the Great Basin crust are examined. Detailed studies of focal mechanisms for several areas in the western Great Basin show a systematic change from strike-slip motion at shallow depths to oblique or normal slip at depth. Explosions detonated in Nevada show asymmetric Rayleigh wave radiation and significant Love wave excitation, usually consistent with a strike-slip mechanism. This has been puzzling in an extensional tectonic environment, where major earthquakes are known to have primarily dip-slip motion. However, it is entirely consistent with our observation that small-to-moderate earthquakes at shallow depth in the western Great Basin are predominantly strike-slip. An explanation for this behavior is provided in terms of rotation of the axis of maximum compressive stress due to increasing overburden pressure with depth.

In section II we present preliminary observations for teleseisms recorded in the vicinity of Hot Creek Valley. Broadband digital recordings were made near the *Faultless* shotpoint for several months period during 1982. Our preliminary analysis indicates that amplitudes vary by more than a factor of two over short distances (5-10 km), however further analysis is required before this can be quantitatively established. Travel time anomaly patterns in a larger region (20-30 km) surounding the *Faultless* shotpoint are being examined using data from the U.S. Geological Network operated in Hot Creek Valley. These show average travel time delays similar to other areas of the Great Basin. Relative travel time delays in the vicinity of the *Faultless* shotpoint are -0.10 relative to the stations in the eastern ranges bounding Hot Creek Valley.

CONTENTS

TECHNICAL REPORT SUMMARY

The research supported by this grant is directed towards the general problems of discrimination and yield estimation. During the past year has evolved along two lines: 1) analysis of stress variation within the crust and its possible effects on "tectonic release"; and 2) effects of large scale mantle structure and crustal focusing/defocusing on parameters such as m_b, trace amplitude, period and t^* over short distances near the *Faultless* shot point.

In section I and appendix A, the effects of stress distribution within the Great Basin crust are examined. Detailed studies of focal mechanisms for several areas in the western Great Basin show a systematic change from strike-slip motion at shallow depths to oblique or normal slip at depth. Explosions detonated in Nevada show asymmetric Rayleigh wave radiation and significant Love wave excitation, usually consistent with a strike-slip mechanism. This has been puzzling in an extensional tectonic environment, where major earthquakes are known to have primarily dip-slip motion. However, it is entirely consistent with our observation that small-to-moderate earthquakes at shallow depth in the western Great Basin are predominantly strike-slip. An explanation for this behavior is provided in terms of rotation of the axis of maximum compressive stress due to increasing overburden pressure with depth.

In section II we present preliminary observations for teleseisms recorded in the vicinity of Hot Creek Valley. Broadband digital recordings were made near the *Faultless* shotpoint for several months period during 1982. Our preliminary analysis indicates that amplitudes vary by more than a factor of two over short distances (5-10 km), however further analysis is required before this can be quantitatively established. Travel time anomaly patterns in a larger region (20-30 km) surounding the *Faultless* shotpoint are being examined using data from the U.S. Geological Network operated in Hot Creek Valley. These show average travel time delays similar to other areas of the Great Basin. Relative travel time

delays in the vicinity of the *Faultless* shotpoint are -0.10 relative to the stations in the eastern ranges bounding Hot Creek Valley.

SECTION I

ESTIMATION OF PRINCIPAL STRESSES AS A FUNCTION OF DEPTH IN THE WESTERN GREAT BASIN

Alan Ryall and Ute Vetter

Surface wave observations require a source with a significant non-isotropic component for some large underground nuclear explosions at both the US and Soviet test sites (Bache, 1982). In early work on this subject, Toksoz and Kehrer (1972a, b) studied Rayleigh wave radiation patterns and Love/Rayleigh amplitude ratios for a number of NTS and Amchitka explosions, and concluded that the non-isotropic or "tectonic release" component was consistent with a strike-slip mechanism. For the USSR, surface waves from some of the eastern Kazakh explosions are more strongly perturbed than has been observed for the US shots (Bache, 1982). Contrary to the NTS model, these observations are consistent with a source mechanism composed of an explosion plus a thrust-fault double couple. For this source Rayleigh-wave phase reversals occur in all azimuths when the seismic moment of the double couple is more than twice the moment of the shot, and in two quadrants when the ratio of the moments is 0.5-2.0.

Archambeau (1981) concludes that non-isotropic components would be expected to perturb explosion signals whenever the shot is detonated in a prestressed medium or in the vicinity of stress-loaded faults. He suggests that the current state of knowledge on tectonic release effects could be considerably expanded by a number of research initiatives, including research aimed at predicting surface-wave perturbations for explosions detonated in "realistic" prestress environments.

In another area of the TBT verification research program, Archambeau

(1982) points out that the capability to identify seismic events in terms of their physical characteristics is fundamental to the discrimination of earthquakes and explosions. "In particular," he states, "one may use the location of the event along with knowledge of the tectonics for the area in which the event has occurred, obtained in part from previously observed earthquakes and in part from other geophysical information including plate tectonics, to infer the most probable (or possible) fault mechanism and hypocentral depth for an event."

As part of our program of research on earthquakes and explosions in the western Great Basin, we have made a detailed investigation of changes in focal mechanism as a function of focal depth. The results of this study indicate that earthquake mechanisms in this region are predictable in terms of epicentral location and depth. Maximum and minimum principal stresses can also be estimated as a function of depth. One significant result of the analysis is that strike-slip mechanisms for shallow earthquakes -- and tectonic release -- at the Nevada Test Site are consistent with the known extensional tectonic regime of the region. Extension of this analysis may provide useful information on prestress environments in regions where other test sites are located.

In a study of earthquakes in central Nevada (Ryall and Vetter, 1982) we observed that events with strike- or oblique-slip mechanisms had average depth of about 7 km, wheras events with normal slip had mean depth of about 12 km. Subsequent analysis of more than 130 earthquakes distributed over most of the western Great Basin show a consistent pattern of primarily strike-slip motion for events shallower than 6 km, while those deeper than 9 km generally have a strong normal-slip component. Figures 1 and 2 illustrate this effect for the Mammoth Lakes area.

In a paper accepted for publication in the *Journal of Geophysical Research* (Appendix A; Vetter and Ryall, 1983) we explain the observed change in mechan-

ism by increasing overburden pressure with depth. Shallower than 6 km the maximum compressive stress is horizontal, leading to strike-slip motion. Deeper than 9-10 km the maximum stres is the overburden pressure, which is vertical. At depths of 6-10 km where the transition takes place the difference between greatest and intermediate principal stress must be small, as indicated by the occurrence of both strike- and oblique-slip events in the 6-9 km range and oblique to normal slip at larger depth. Our observations, together with measured stress in crustal rocks (Sibson, 1974; Byerlee, 1977; Zoback and Zoback, 1980; McGarr, 1980) can be used to roughly estimate the principal stresses at greater depth, as illustrated by Figure 3. Within the western Great Basin we find the maximum and minimum compressive stress at depth of 3 km to be about 104 and 55 MPa, respectively. At depth of 20 km the maximum stress is vertical and equal to the overburden pressure, about 530 MPa; the minimum stress is horizontal and about 260-300 MPa.

Our observations also indicate that the fault-plane dips decrease with depth, but the change from strike- to dip-slip motion is not consistent with listric faulting such as observed in the eastern Great Basin. Instead, based on a model proposed by Hill (1977) to explain the predominance of strike-slip mechanisms in geothermal areas, we suggest that lithospheric extension in the western Great Basin may occur through oblique or normal faulting at mid-crustal depths and the formation of vertical fissures or magma-filled dikes at shallow depth. A model for the shallow earthquakes in the Mammoth Lakes area is shown on Figure 4.

References

Archambeau, C. B. (1981). Tectonic generation, in *A Technical Assessment of Seismic Yield Estimation, Appendix, Part 2*, DARPA-NMR-81-01.

Archambeau, C. B. (1982). Discrimination based on physical parameter estimation of seismic sources, *DARPA Symposium on Seismic Detection, Analysis, Discrimination and Yield Determination*, DARPA-GSD-8201, 19-25.

Bache, T. C. (1982). Estimating the yield of underground nuclear explosions, *Bull. Seism. Soc. Am.*, *72*, S131-S168.

Byerlee, J. (1977). Friction of rocks, *US Geol. Survey, Open-File Rpt, Experimental Studies of Rock Friction with Application to Earthquake Prediction*, 55-77.

Hill, D. P. (1977). A model for earthquake swarms, *Jour. Geophys. Res.*, *81*, 745-754.

McGarr, A. (1980). Some constraints on levels of shear stress in the crust from observations and theory, *Jour. Geophys. Res.*, *85*, 6231-6238.

Ryall, A. and U. R. Vetter (1982). *Seismicity Related to Geothermal Development in Dixie Valley, Nevada*, Final Rpt. on USDOE Contract DE-AC08-79NV10054, Univ. of Nevada, Reno, 102 pp.

Sibson, R. H. (1974). Frictional constraints on thrust, wrench and normal faults, *Nature*, *249*, 542-544.

Toksoz, M. N. and H. H. Kehrer (1972a). Tectonic strain release by underground nuclear explosions and its effect on seismic discrimination, *Geophys. J.*, *31*, 141-161.

Toksoz, M. N. and H. H. Kehrer (1972b). Tectonic strain release characteristics of CANNIKIN, *Bull. Seism. Soc. Am.*, *62*, 1425-1438.

Vetter, U. V. and A. S. Ryall (1983). Systematic change of focal mechanism with depth in the western Great Basin, *Jour. Geophys. Res.*, in press.

Zoback, M. L. and M. D. Zoback (1980). State of stress in the conterminous United States, *Jour. Geophys. Res.*, *85*, 6113-6156.

Figure Captions

Figure 1. Locations and fault-plane solutions for Mammoth Lakes earthquakes with depth less than 9 km.

Figure 2. Locations and fault-plane solutions for Mammoth Lakes earthquakes with depth greater than 9 km.

Figure 3. Estimated principal stresses as a function of depth. P_0 -- hydrostatic pore pressure, $S_1 - S_3$ -- twice the maximum shear stress measured for hard rocks and extrapolated downwards, $S_h = S_3$ -- smallest horizontal principal stress, S_v -- overburden pressure, S_H -- greatest horizontal principal stress.

Shaded area shows range of S_3. Points with numbers are described in the text.

Figure 4. Model to explain strike-slip faulting for shallow Mammoth Lakes earthquakes. Top left - Rose diagram showing orientation of T-axis; tope right - Rose diagram showing stike of the two planes of the fault-plane solutions; bottom - model with vertical fissures (dikes) forming together with conjugate right- and left-lateral shears on planes shown.

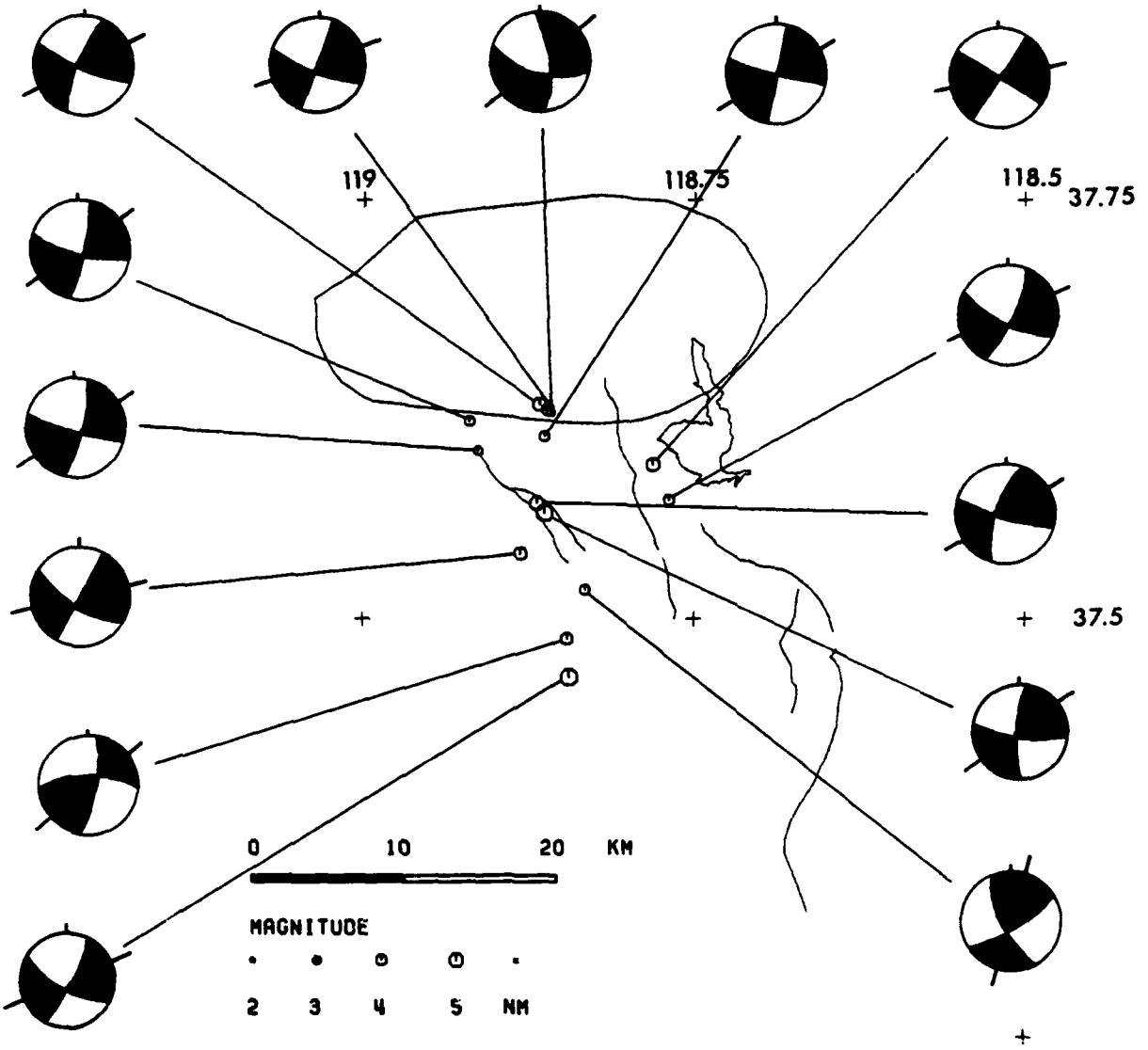

Figure 1.

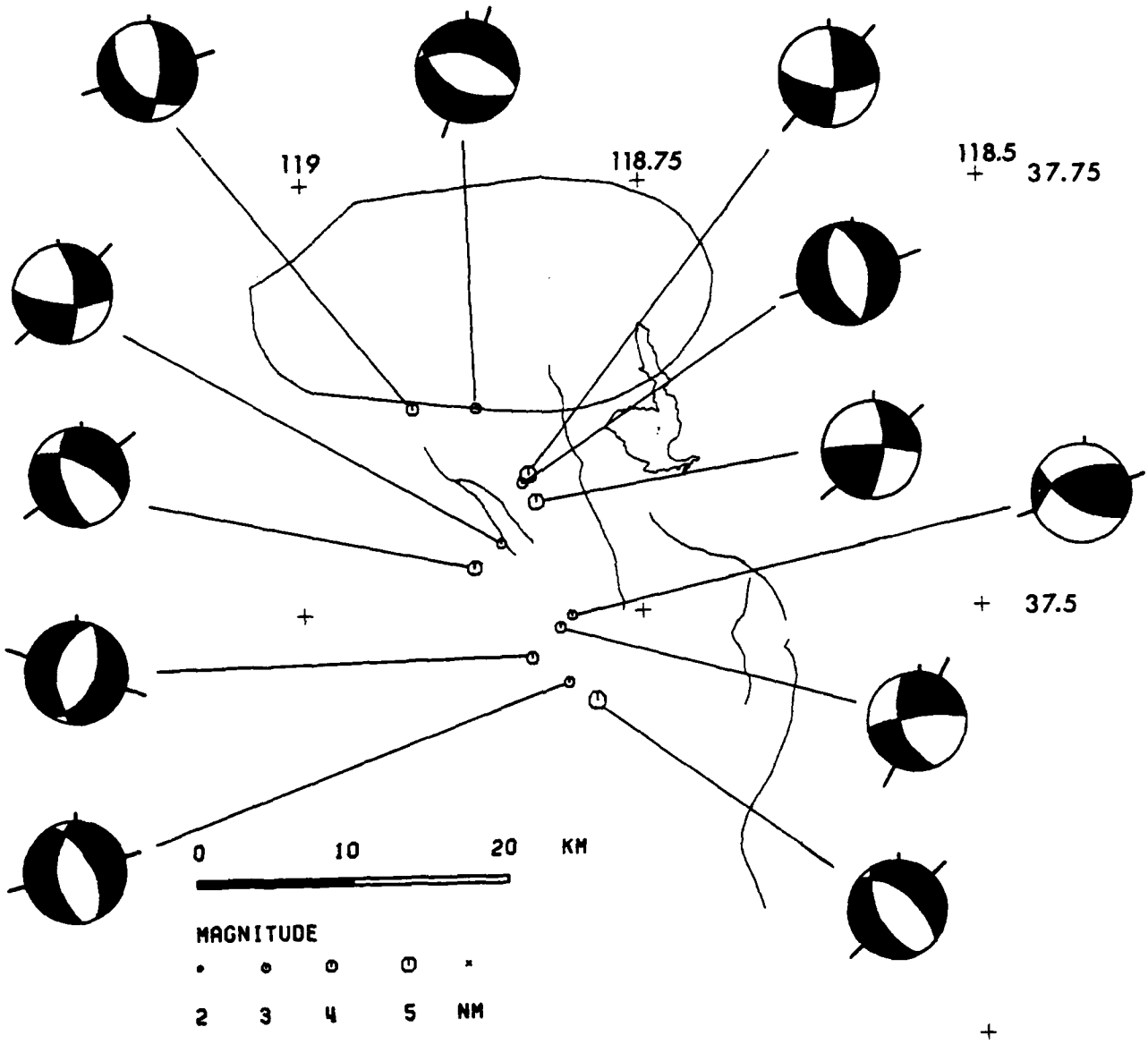

Figure 2.

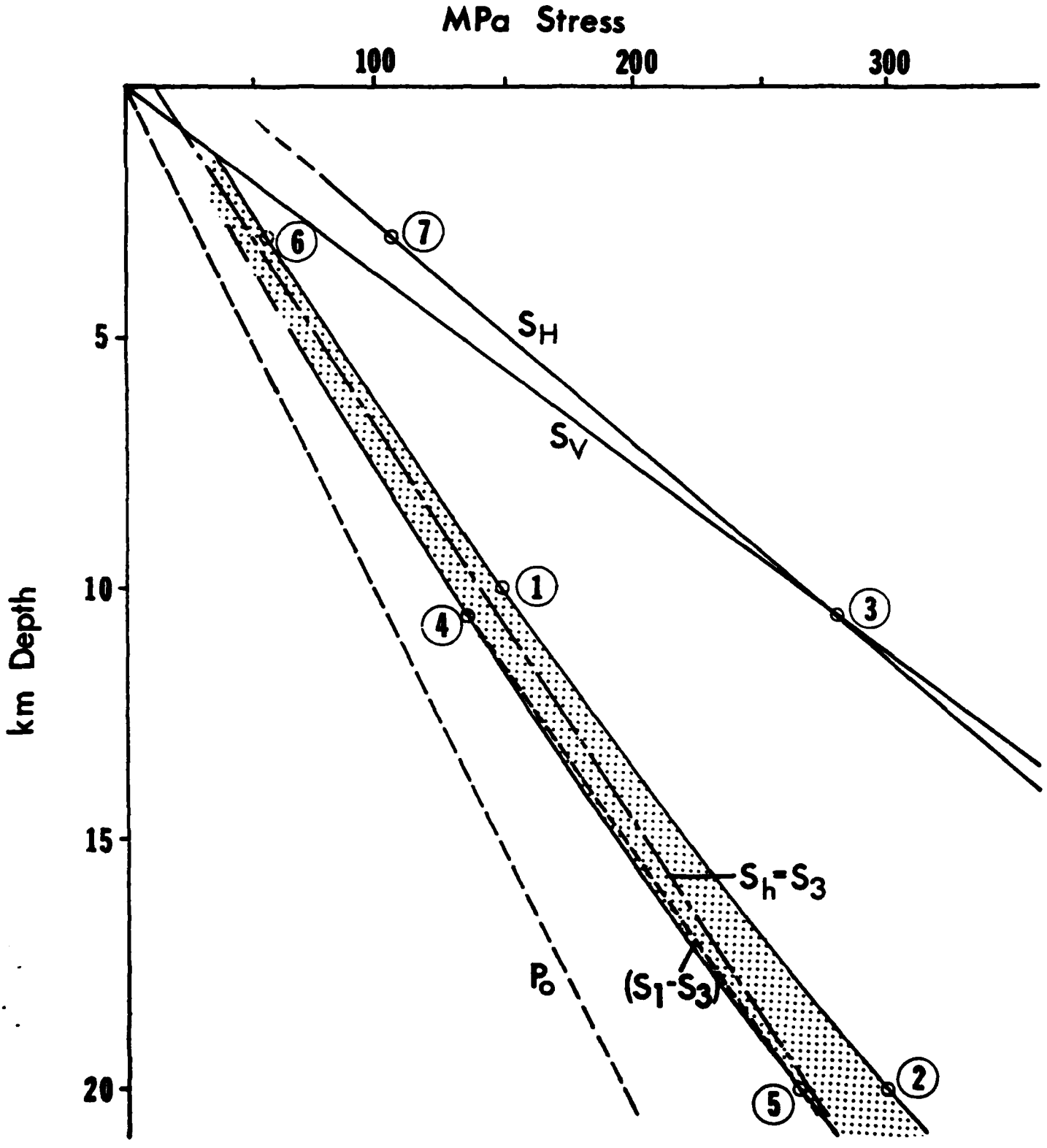
MPa Stress
100
200
300
km Depth
5
10
15
20
S_H
S_V
S_h=S_3
P_o
(S_1-S_3)
1
2
3
4
5
6
7

Figure 3.

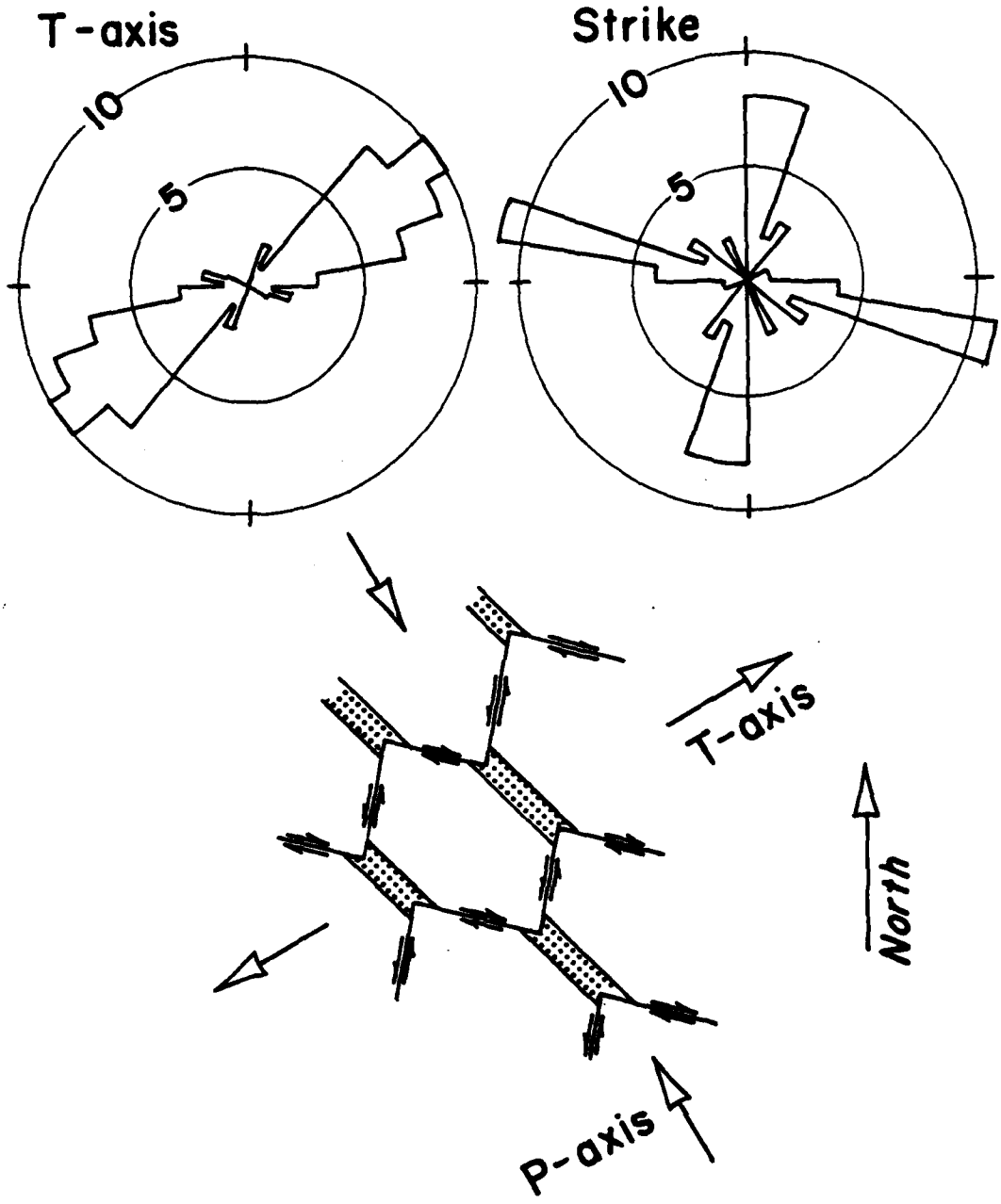

Figure 4.

SECTION II

Teleseismic observations in the vicinity of the Faultless test site

Keith Priestley

Introduction

With the current emphasis on TTBT, improving the accuracy of yield determination to verify treaty compliance has given new importance to the problems of magnitude bias and regional differences in attenuation. As pointed out by Bache *et al*,(1981) and Bache(1982), while it is generally accepted that there exist broad regional (i.e., WUS, EUS) differences in attenuation, there are still obstacles to accurate prediction of amplitude variations at individual stations within these regions. In a study of amplitude and m_b bias at LASA, Chang and von Seggern (1980) found fluctuations of about 0.15 m_b in standard deviation among the subarrays, even after determining azimuthal corrections. Detailed modeling could not identify the source of the bias (azimuthal effect, subarray effect or azimuth-subarray interaction), and the authors concluded that both amplitude and traveltime anomalies might be due to local focusing/defocusing effects in the crust. The authors concluded that "in a region as complex as LASA", – a region originally selected for its geologic *uniformity* (Green *et al.*, 1966), – a factor of 2 in uncertainty results for predictions of a station's amplitude for a hypothetical event only 50 km away from a hypothetical calibration shot.

In a recent SDCS experiment, Teledyne-Geotech installed and operated high-quality short-period stations at WUS test sites, and compared the recorded

teleseismic signals with data from RKON and two stations in Maine (Der *et al.*, 1981). Scatter in the data was large for station pairs with 10-20 km spacing. At NTS the standard deviation of relative magnitude differentials was 0.2-0.3 m_b. However, with appropriate corrections for crustal structure, the NTS differentials could be reduced to a few hundredths of a m_b unit. After correction, m_b differentials between Great Basin test sites (NTS, *Faultless* site, *Shoal* site) and RKON still ranged from 0.16 to 0.44 m_b. Such large differences were not observed for t^* differentials computed for pairs of stations by spectral ratios—the spread for 12 WUS stations was only about ±0.05, while the difference between RKON and the WUS t^* values was 0.20. In agreement with the study by Cahng and von Seggern, Der *et al* suggested that t^* differentials reflect true regional differences in anelastic attenuation, while the large scatter in m_b and trace amplitude measurements within the WUS may be the result of local focusing effects.

One of the sites of interest is Hot Creek Valley (CNTA), in central Nevada, the location of the *Faultless* test of January 19, 1968. The ISC gave the *Faultless* explosion a teleseismic body-wave magnitude of 6.3 based on 44 readings. This is more than 0.3 m_b units greater than the estimated maximum magnitude (Evernden, 1971) of the device based on the announced yield range of 200 kt - 1 Mt (Springer and Kinnamann, 1971) indicating that CNTA has low attenuation relative to NTS. However the Teledyne-Geotech study (Der *et al*, 1981) of SDCS teleseismic data indicates that relative to NTS, CNTA is a high attenuation site, thus presenting an apparent violation of reciprocity.

Geologic Setting

Hot Creek Valley in central Nevada is a region of extensive, late Cenozoic volcanism. The volcanic deposits of the Lunar Craters area in southern Hot

Creek Valley have been studied by Scott and Trask (1971). The volcanic field includes cinder cones, maars, and basalt flows of probable Quaternary age.

Structures in this region are relatively simple and are reflected by the physiography typical of the Basin and Range province (Figure 1). Folding, where present, is mild, and numerous normal faults separate blocks which are tilted generally eastward. In places, this picture is made more complex by large masses of Paleozoic rocks that have slid or been thrust over the Tertiary ignimbrites.

The Quaternary basalt flows, cinder cones, and craters are underlain and partly surrounded by Tertiary rhyolite tuffs and flows, and Paleozoic carbonate rocks. Basalt flows and cinder cones of Miocene age are the most widespread of all the deposits and extend from the northern to the southern edge of the volcanic field. There is little infilling of the most recent crater, and the flanks of the cone are not gullied by erosion. The crater rims have remained relatively sharp, and loose ejecta form a slope of 35°, a maximum for cones in this area, indicating a very young age (at most several thousand years).

Basalt flows, cinder cone chains, mounds, craters, and fissures rimmed with pyroclastic ejecta were produced along normal faults and fissures resulting from regional extension that started about 17 m.y ago, and has continued to the present. At least three episodes of late volcanism occurred throughout the volcanic field, separated by brief periods of relative dormancy. These interludes may not have been distinct and probably represent overlapping pulses of activity. Each episode began with the eruption of pyroclastic material that formed small mounds; as these grew larger and became cone shaped, the initial extrusion of highly vesicular basalt flows and ejecta produced composite or mixed volcanic structures. This early explosive phase probably resulted from a combination of the high volatile content of the magma and greater amount of

ground water available at the onset of volcanism. In the final stages, as magma continued to rise in the vents, many cones were breached where the lavas overflowed or eroded the walls of cinders and ashes. The weakness of the ringwalls was apparently conditioned by linear fissures and faults along which the cones developed, as shown by the preferred northeast-southwest orientation of the ruptures.

Digital recordings

To aid in explaining the apparent discrepency in the amplitude of outgoing vs. incoming waves, the University of Nevada moved a digital array previously operating in the Catskill Mountains, New York, (Pomeroy, 1980) to Hot Creek Valley in mid-January, 1982. The locations of the stations are shown in figure 1. The site labled *GROUND ZERO* is at the *Faultless* shotpoint; the station labled *MOREY MINE* is in competent rhyolitic rocks in the range 5 km to the west of *GROUND ZERO*; the station labled *NEEDLES* is in volcanic flows 10 km east of *GROUND ZERO*. The stations were installed to study variations in such parameters as m_b, trace amplitude, period and t* over short distances within the vicinity of the *Faultless* shot point, and to determine to what extent these variations can be explained by large structures within the mantle (e.g., high-velocity zones such as proposed under NTS calderas by Spence, 1974), or by local focusing/defocusing within the crust (e.g., such as the crustal inhomogeneities at LASA proposed by Chang and von Seggern, 1980).

Several unanticipated problems developed which limited the scope of this experiment. Most critical of these problems involved transmitting the seismic data from the remote stations to the central recording site. As the array was operated in New York, data was transmitted from stations to recording site via leased telephone lines, something not possible in remote areas of Nevada. Thus

the system was modified to employ VHF radios. The Seismological Laboratory technical staff have had a great deal of experience with VHF transmission of seismic data over the past eight years and anticipated no problems with the relatively short transmission paths involved in Hot Creek Valley. However, we experienced a great deal of intermittent radio interference especially in the path from ground zero to the central recording site. At times, three watt radios were insufficient over short (15-20 km) line-of-site paths, while the technical personnel were simultaneously maintaining visual contact. We have not experienced similar interference at any other sites in western Nevada and suspect that the interference may result from the Air Force installations in the valley and surrounding ranges. Thus, over much of the seven months of operation, data were received from the remote sites only intermittantly.

Other problems included poor environmental controls for the recording computer facility (heat, dust, power fluctuations, lightning), and inexperienced local personnel.

Much time during the past year has involved writing and assembling software for playing back and processing the digital data. We have made a preliminary analysis of the two seismograms shown in Figure 2. In both instances the amplitude observed at the "ground zero" site are significantly larger than those observed at the two stations sited on rock. All stations were operating at the same magnification and hence the amplitude variations shown in the time series between components for an event represents real variations in amplitude between the three sites. No corrections have been made for site amplification resulting from differences in sediment thickness beneath each site.

Both events were from the northwest, and both, qualitatively show a high degree of phase coherence over the first several cycles of the P-wave on all components. The first event is larger resulting in a higher signal to noise ratio. All

three north-south components for this event show a strong phase following the P onset by 5.6 ±02 seconds. This may be a P to S conversion at a boundary beneath the array. The average P and S wave velocities for the Great Basin crust are 6.27 and 3.65 k/s respectively (Hill and Pakiser, 1967; Priestley and Brune, 1978). If the observed phase is assumed to be a P to S conversion at the base of the crust, the boundary occurs at a depth of about 49 km. This is deeper than the Moho depth postulated within east-central Nevada from refraction (37 km, Eaton, 1963; 38 km, Hill and Pakiser, 1967; 35 km, Priestley *et al*, 1982). The average P and S wave velocities for the entire lithosphere are 8.96 and 4.04 k/s, respectively (Burdick and Helmberger, 1978; Priestley and Brune, 1978). If the conversion is assumed to occur at the base of the lithosphere the boundary occurs at 54 km depth, less than the average depth for the base of the lithosphere from published body wave (65 km, Burdick and Helmberger, 1978) and surface wave (64 km, Priestley and Brune, 1978) studies. This postulated converted phase is apparent on only one of the two events examined to date.

Figure 3 shows a comparison of the power spectra of the vertical component seismograms for the two events. The sample rate of the data is 25 samples/second, and the time window taken is the first 10.24 seconds of the P-wave. To estimate the noise level, 10.24 seconds of the time series preceding the P-onset were analyzed in the same manner as the P-wave. For both events, the amplitude of the signal at 1 Hz observed at station "Ground Zero" is significantly larger than that observed at the other sites. Instrument and site corrections need to be made before a more quantitative statement can be made concerning local effects on m_b estimates.

Teleseismic P-delays at Hot Creek Valley

Evernden (1977) summarized past studies of station magnitude bias, and found that magnitude bias can be correlated with travel time anomalies, crustal thickness under the station, a low-velocity channel in the upper mantle, high heat flow, and upper mantle velocity structure. Chang and von Seggern (1980) found that amplitude anomalies at LASA are linearly related to the amount of travel time anomaly, implying that both effects are due to a similar cause, which they suggest to be crustal focusing. With this in mind, we have begun an analysis of teleseismic P-wave delays in the vicinity of the *Faultless* shotpoint in Hot Creek Valley. From late September, 1969 through September, 1970, the U.S. Geological Survey operated seven short-period seismograph stations in and around Hot Creek Valley. Each station was equipped with a vertical component, short-period (1 Hz) seismometer. The signals were telemetered to a central recording site and recorded along with WWVB time code on 16 mm develocorder film. With the common time base, clock corrections are unnecessary. The station locations are shown in figure 1.

Teleseismic P-wave arrival times have been read directly from the develocorder films for 41 events in the distance range 25° to 100°. Most events were from the southwest Pacific, the Japan-Aleutian arc, or Central and South America; however, a number of events were included from Europe and the mid-Atlantic rise. The quality of the data varied significantly depending on the amplitude of the arrivals and the level of instrumental noise. In general, the waveforms showed a high degree of coherency across the network. Often one or more stations were inoperative and data were only included in the analysis for which recordings were available for at least four stations.

A total of 272 arrival times have been read of coherent phases across the array. Occasionally the first arrival time was read, but more often the time of

the first peak or trough was read. Readings were made to a precision of 0.01 second. To account for the uncertainties due to noise, the phase times were bracketed by the time for which we could determine with a high degree of certainity that the phase had not arrived, and the time for which we were certain that the phase had arrived. The error bounds varied from ±0.02 seconds for impulsive events during quiet intervals, to ±0.15 seconds for weaker arrivals during more noisy intervals. Typically the error bounds were approximately ±0.05 seconds.

Elevation corrections were applied to the data correcting the arrival times to those which would have been recorded at the *Faultless* shot point elevation. In general this elevation change was small (i.e. the maximum elevation change was 1328m). Thus significant errors should not be introduced into the data due to the wrong choice of velocity for the surficial layer. Absolute P wave residuals were calculated with respect to the Herrin travel-time tables (Herrin, 1968) using the event location and origin times from the Preliminary Determination of Epicenter bulletins. Relative residuals were then recorded for each station with respect to the weighted mean travel time residual, i.e.

$$R_{ij} = R^H_{ij} - \frac{1}{N}\sum_{i=1}^{N} W_{ij} R^H_{ij}$$

where R_{ij} is the relative residual for the i^{th} event at the j^{th} station, R^H_{ij} is the residual compared to the theoretical Herrin travel times, N is the number of stations recording the i^{th} event, and W_{ij} is a weighting factor for the i^{th} event at the j^{th} station. Not all stations recorded every event, therefore the weighted mean travel time may be computed by a different subset of stations for various events.

The average travel time difference across the seven stations is greater than 2 seconds, typical for the Great Basin. The pattern of individual station residu-

als relative to this average roughly correlates with the geologic patterns in the vicinity of the stations. The average station residuals in seconds are shown on Figure 1. Station CNBC is located in the valley center and shows the largest positive residual (0.23 sec), presumably resulting from the slower velocity valley sediments. The stations along the eastern ranges (CNEC, CNHM, CNSB, and CNPS) all show small residuals (-0.02±0.02 sec). The stations along the western range (CNHC and CNHR) show larger negative residual (-0.10 sec).

Figure 4 shows the distribution of relative residuals with azimuth and on an equal-area lower-hemisphere stereographic projection. Station CNBC has all positive residuals and shows no obvious azimuthal trend. Stations CNHM and CNEC generally show positive relative residuals for waves approaching at steep angles from the southeast, and negative residuals for waves approaching from the southwest. Station CNHR and CNHC, both located on the west side of the valley, have negative residuals (with a few exceptions to the southeast), with no apparent azimuthal trend. Station CNSB has mainly positive residuals for most azimuths, with the largest residuals for the southern quadrant. Station CNPS shows the strongest azimuthal trend, with positive residuals for waves approaching from the north or south, and negative residuals for waves approaching from the east or west. For all stations, waves approaching from the southeast, the azimuth of the recent volcanism, show the largest relative delays, although each station has its own azimuthal pattern. We are currently timing the last six months of data from the U.S. Geological Survey network and expect that the remaining data will help clarify the underlying cause of the delay pattern.

To supplement the teleseismic recordings in Hot Creek Valley, teleseismic travel time residuals have also been computed from recordings of the *Faultless* explosion. Arrival times were taken from the ISC bulletin, using only those arrivals which were read to the nearest 0.1 second, which showed an ISC residual

of less than 5.0 seconds, and for which P-wave station corrections were available (Dziewonski and Anderson, 1983). Travel time residuals were computed as above relative to CNHC. The travel time data from *Faultless* show fast travel times, with the fastest travel times to the northeast. These travel times are more negative than the surface receivers. The *Faultless* explosion was detonated well below the valley fill in saturated tuff, and therefore is not affected by the sediment delays as are the surface receivers. The relative travel time advance for *Faultless* suggest the possible existence of high velocity, shallow mantle material beneath the Tertiary volcanic center. Spence (1974) has reported a similar observation associated with the Silent Canyon Caldera at the Nevada Test Site. The required velocity difference beneath the cauldron compared to more "typical" Great Basin mantle material, is within the range predicted by Jordan (1979), which would result from compositional variation in the upper mantle associated with basaltic differentiation.

REFERENCES

Bache, T.C., W.J. Best, R.R. Blandford, G.V. Bulin, D.G. Harkrider, E.J.Herrin, A. Ryall, and M.J. Shore (1981). A technical assessment of seismic yield estimation, DARPA- NMR-81-02, Defense Advance Research Projects Agency, Arlington, Virginia.

Bache, T.C., (1982). Estimating the yield of underground nuclear explosions, *Bull. Seismo. Soc. Am., 72 Part B*, p131-168.

Burdick, L.J., and D.V. Helmberger, (1978). The upper mantle P velocity structure of the western United States, *J. Geophys. Res., 83*, 1699-1712.

Chang, A.C., and D.H. von Seggern (1980). A study of amplitude anomaly and m_b bias at LASA subarrays, *J. Geophys. Res., 85*, 4811-4828.

Der, Z.A., T.W. McElfresh, and A. O'Donnell (1983). An investigation of the regional variations and frequency dependence of anelastic attenuation in the mantle under the United States in the .5-4 Hz band, Submitted to the *Geophys. J.R. astr. soc.*

Dziewonski, A. and D. Anderson, (1983). Travel times and station corrections for p-waves at teleseismic distance, submitted to *J. Geophys. Res.*

Eaton, J.P., (1963). Crustal structure from San Francisco, California, to Eureka, Nevada, from seismic refraction measurements, *J. Geophys. Res., 68*, 5789-5806.

Everden, J. (1971). Magnitude versus yield of explosions, *J. Geophys. Res., 75*, 1028-1032.

Evernden, J.F. (1977). Regional bias in magnitude versus yield measurements: Its explanation and mode of evaluation, written communication.

Green, P.E., R.A. Frosch, and C.F. Romeny (1965). Principles of an experimental large aperture seismic array (LASA), *Proc. of IEEE, 53*, 1821-1833.

Herrin, E. (1968). 1968 seismological tables for P phases, *Bull. Seismo. Soc. Am., 58*, 1193-1241.

Hill, D., and L. Pakiser (1966). Crustal structure between Nevada Test Site and Boise, Idaho, in *The Earth Beneath the Continents: Am. Geophys. Union, Geophys. Mon., 10*, 391-419.

Jordan, T. (1979). Mineralogies, densities and seismic velocities of garnet iherzolites and their geophysical implications, in *The Mantle Sample: Inclusions in Kimberlites and Other Volcanics*, edited by F.R. Boyd and H.O.A. Meyer, pp 1-14, AGU, Washington, D.C.

MacDonald, G.A. (1969). Composition and origin of Hawaiian lavas, in studies in vulcanology—a memoir in honor of Howel Williams: *Geol. Soc. America Mem., 116*, 477-522.

Pomeroy, P.W. (1980). Seismic discrimination at regional distances, Annual Technical Report, AFOSR Contract #F49620-80-C-0021

Priestley, K.F., and J.N. Brune (1978). Surface waves and the structure of the Great Basin of Nevada and western Utah, *J. Geophys. Res., 83*,2265-2272.

Priestley, K.F., A.S. Ryall, G.S. Fezie (1982). Crustal and upper mantle structure in the northwest Basin and Range Province, *Bull. Seismo. Soc. Am., 72*, 911-923.

Scott, D.H. and N.J. Trash (1971). Geology of the lunar crater volcanicfield, Nye County, Nevada: U.S. Geol. Survey Prof. Paper 599-I, 22p.

Spence, W. (1974). P-wave residual differences and inferences on an upper mantle source for the silent canyon volcanic centre, southern Great Basin, Nevada, *Geophys. J.R. astr. Soc., 38*, 505-523.

Springer, D.L. and R.L. Kinnaman (1971). Seismic source summary for U.S. under ground explosions, 1961-1970, *Bull. Seismo. Soc. Am., 61*, 1073-1098.

FIGURE CAPTIONS

Figure 1. Location map of Hot Creek Valley in the vicinity of the *Faultless* shotpoint. Stations CNBC, CNEC, CNHM, CNHR, CNHC, CNSB, and CNPS denote U.S. Geological Survey stations, data from which are being used in the P-delay study. The average relative delay is given following the station designation. Stations MOREY MINE, GROUND ZERO, and NEEDLES denote University of Nevada digital stations, data from which are being used in the waveform and amplitude studies. The darkest geologic units in the vicinity of CNEC and southward denote recent volcanic deposits.

Figure 2. Digital seismograms of the two events discussed in the text.

Figure 3. Comparison of the power spectra for vertical component seismograms shown in figure 2.

Figure 4. Left - Relative, teleseismic P-wave residuals as a function of azimuth; right - Relative residuals on equal area lower hemisphere stereographic projections; (¨)+0.05→+0.15 sec, (·)+0.04→−0.04 sec, (▵)−0.05→−0.15 sec.

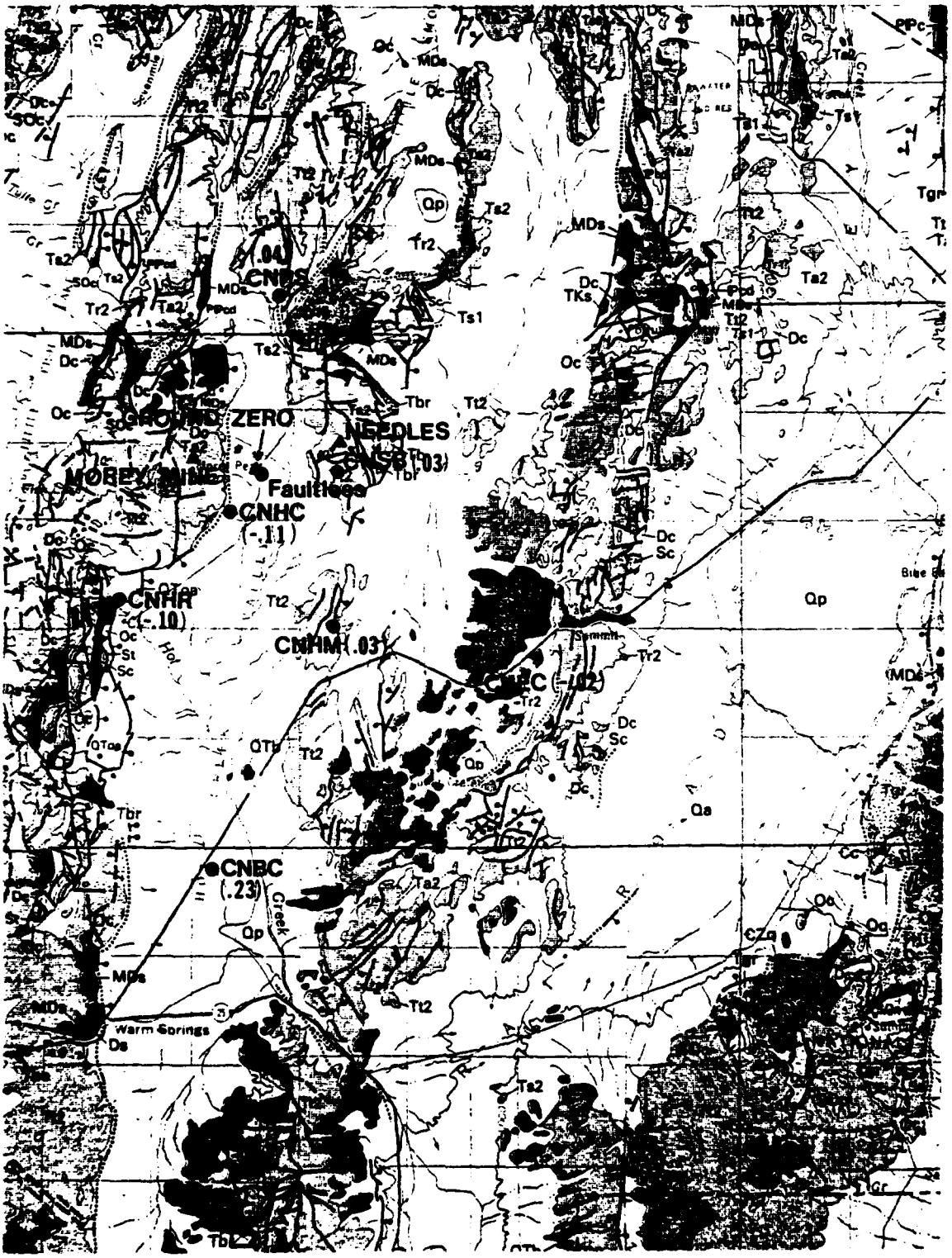
ZERO
NEEDLES
Faultless
CNHC
(-.11)
CNHR
(-.10)
CNHM (.03)
CNBC
(.23)
Warm Springs
Qp
Qa
MDs
Tt2
Ts2
Tr2
Ta2
Tbr
Dc
Sc
Oc

Figure 1.

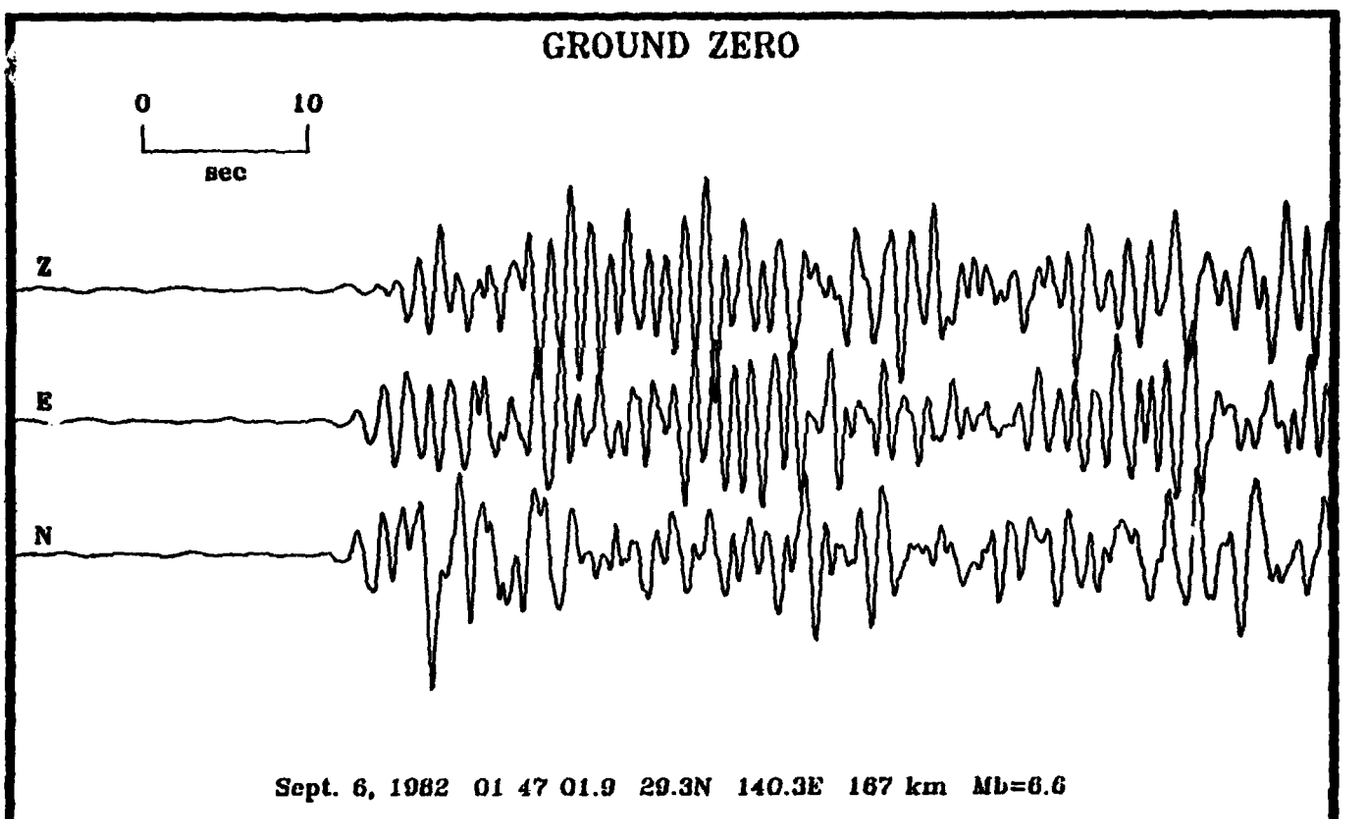
GROUND ZERO
0
10
sec
Z
E
N
Sept. 6, 1982 01 47 01.9 29.3N 140.3E 167 km Mb=6.6

Figure 2a.

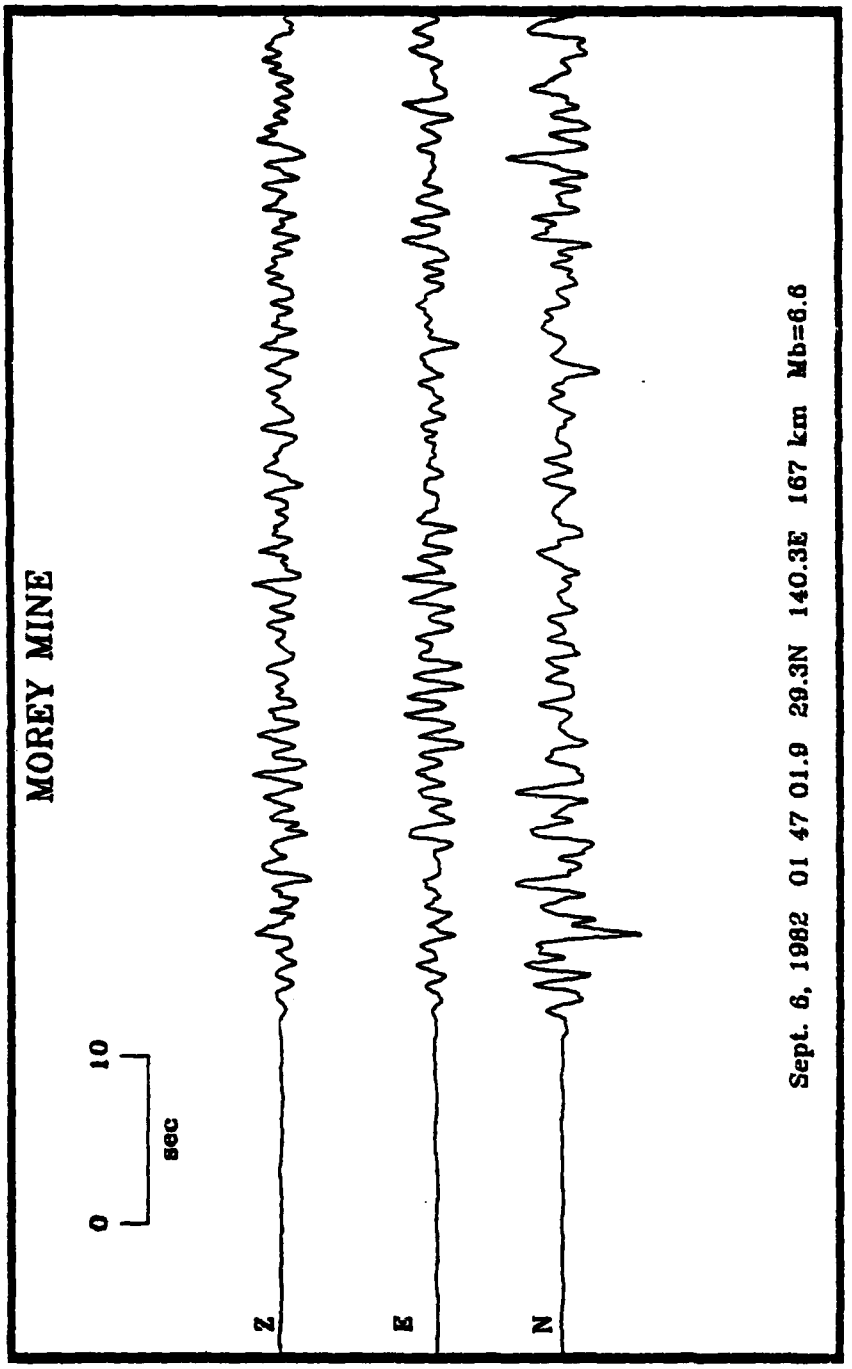
MOREY MINE
0
10
sec
Z
E
N
Sept. 6, 1982 01 47 01.9 29.3N 140.3E 167 km Mb=6.6

Figure 2b.

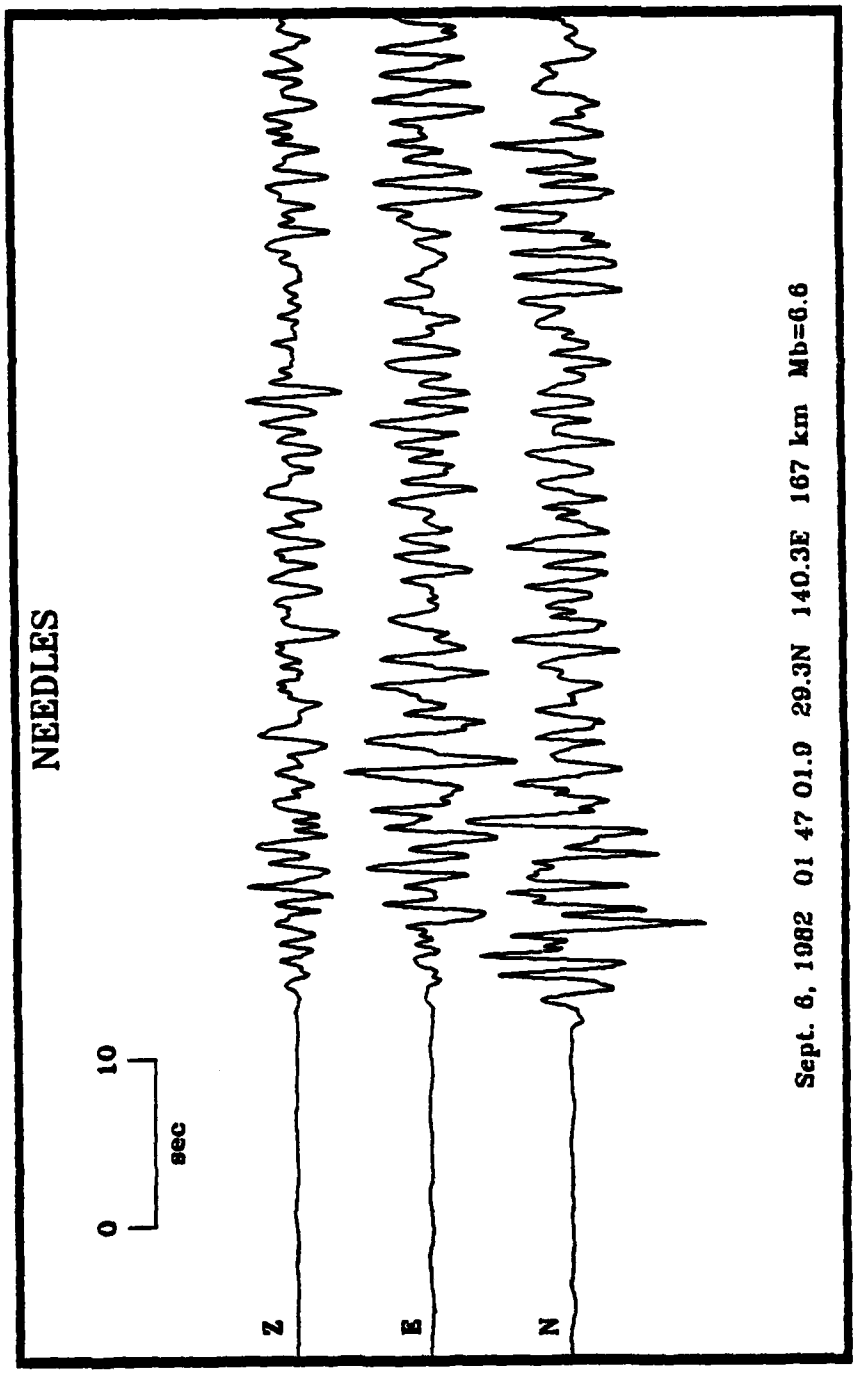
NEEDLES
0
10
sec
Z
E
N
Sept. 6, 1982 01 47 01.0 29.3N 140.3E 167 km Mb=6.6

Figure 2c.

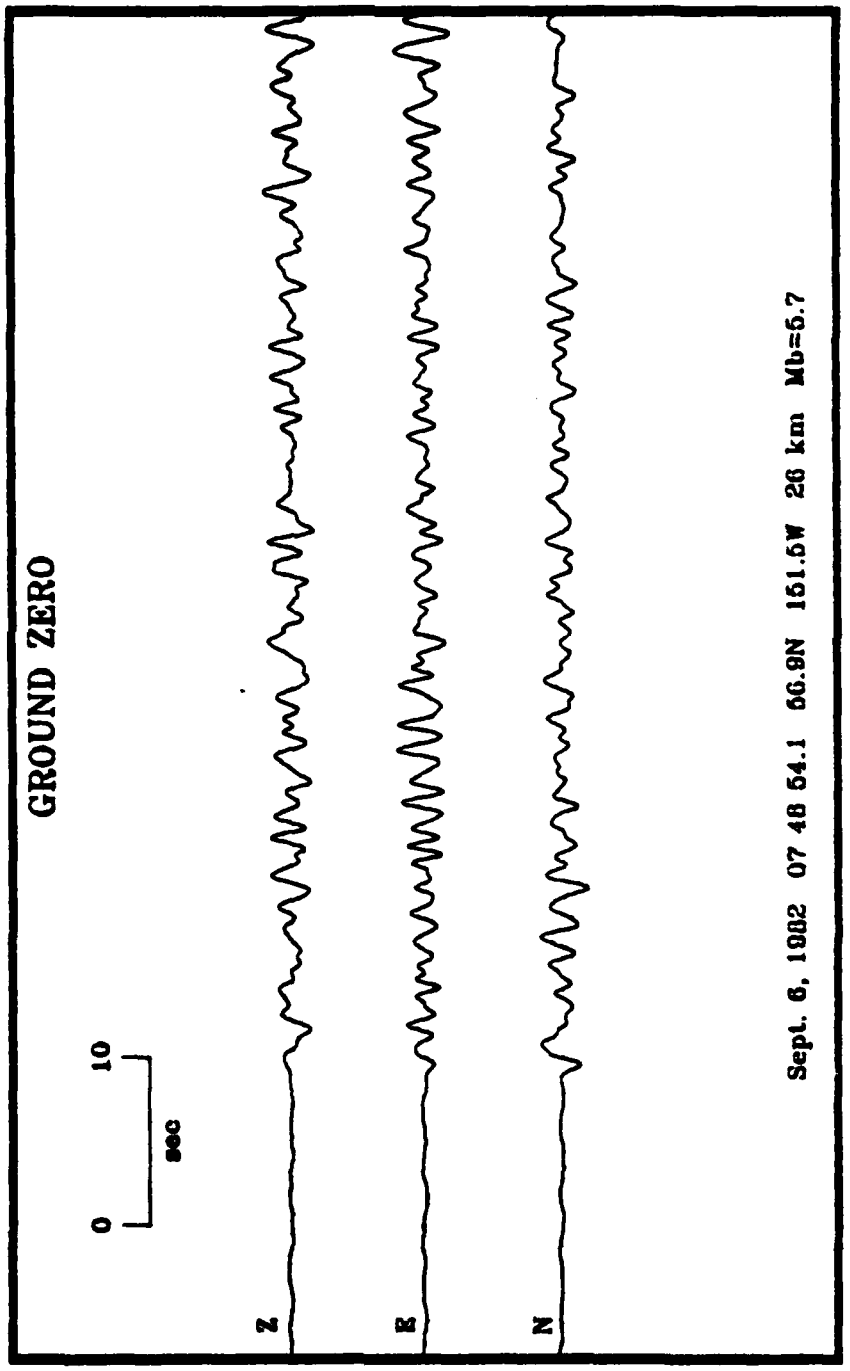
GROUND ZERO
0
10
sec
Z
E
N
Sept. 6, 1982 07 48 54.1 66.9N 151.5W 26 km Mb=6.7

Figure 2d.

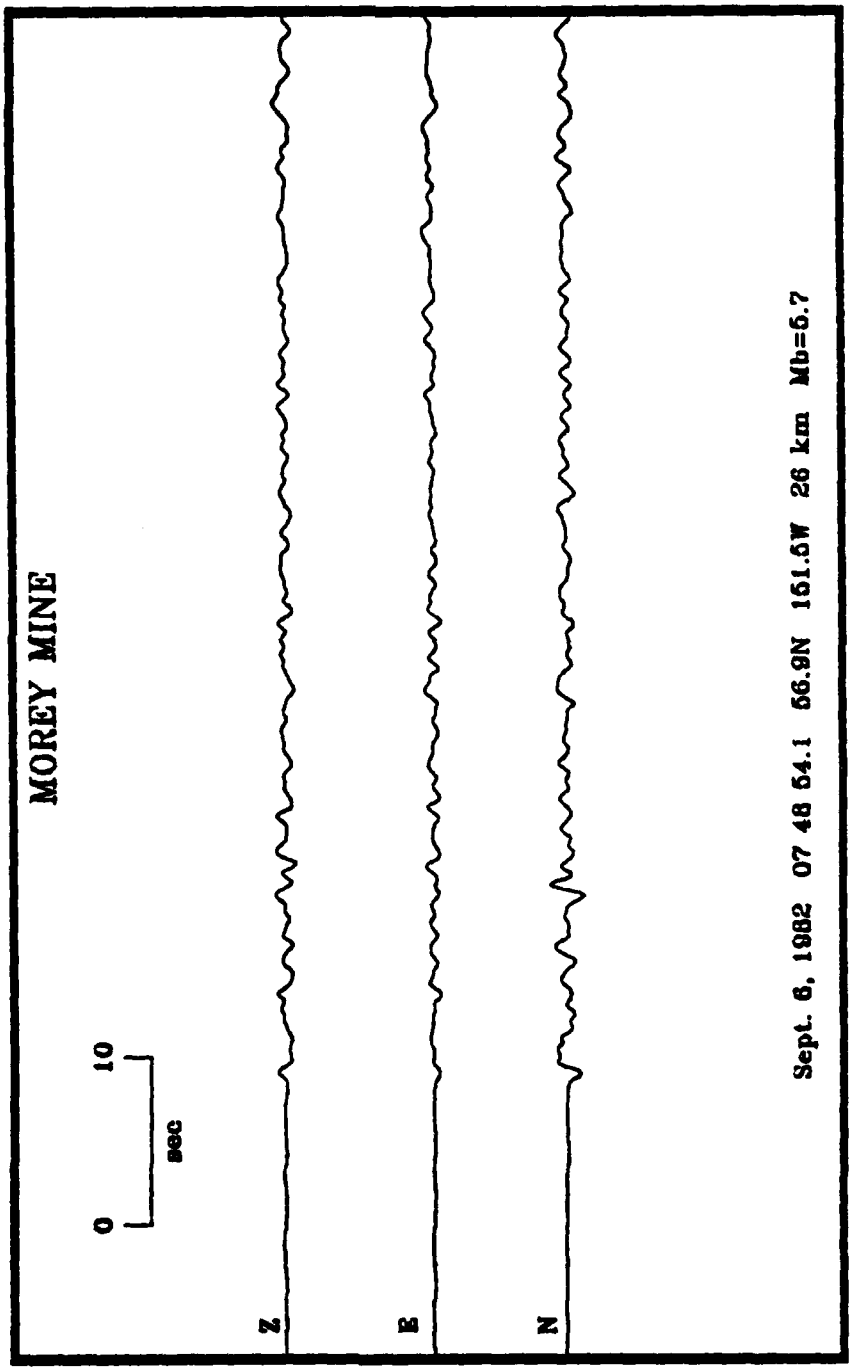
MOREY MINE
0
10
sec
Z
E
N
Sept. 6, 1982 07 48 54.1 56.9N 151.5W 26 km Mb=5.7

Figure 2e.

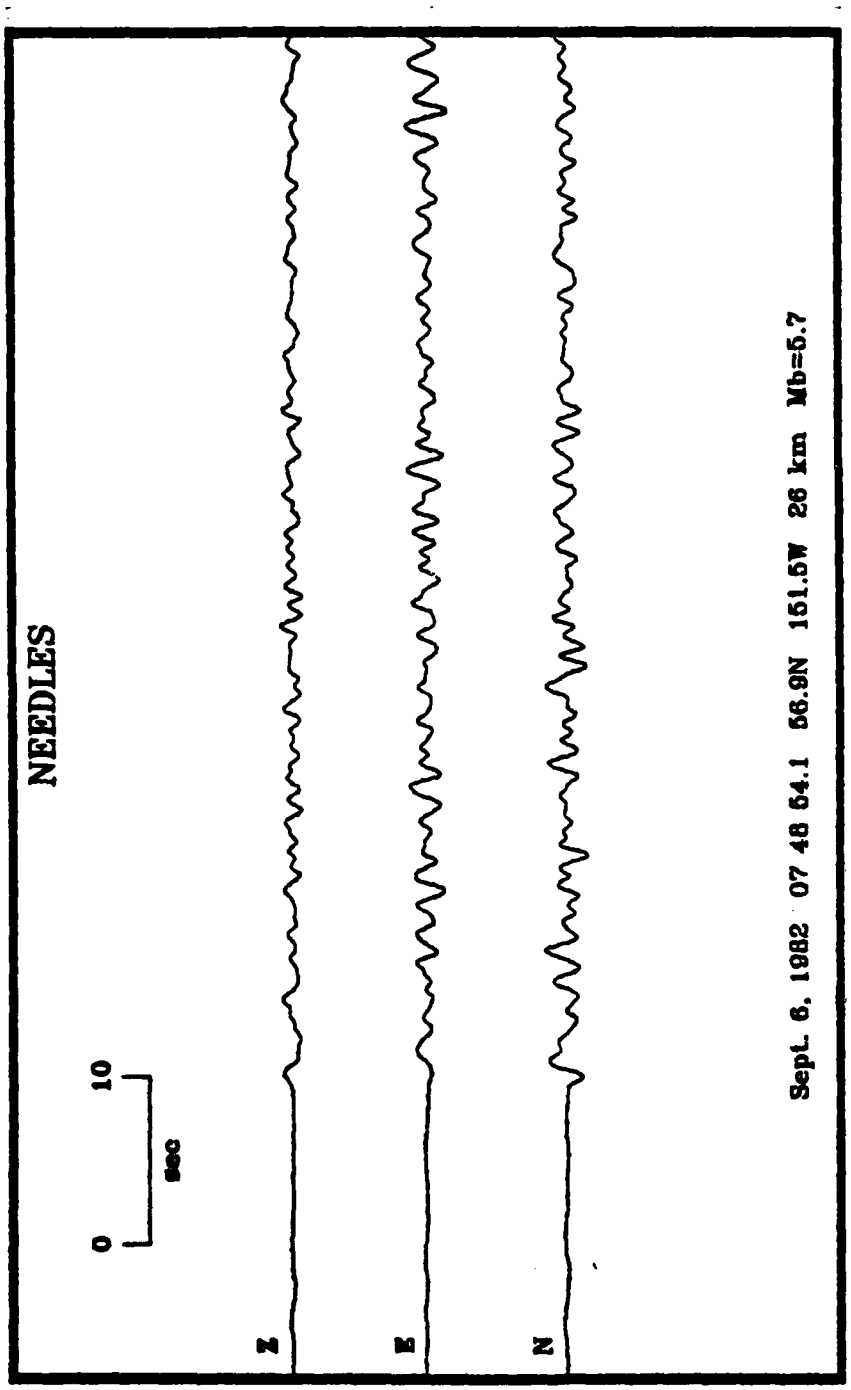

Figure 2f.

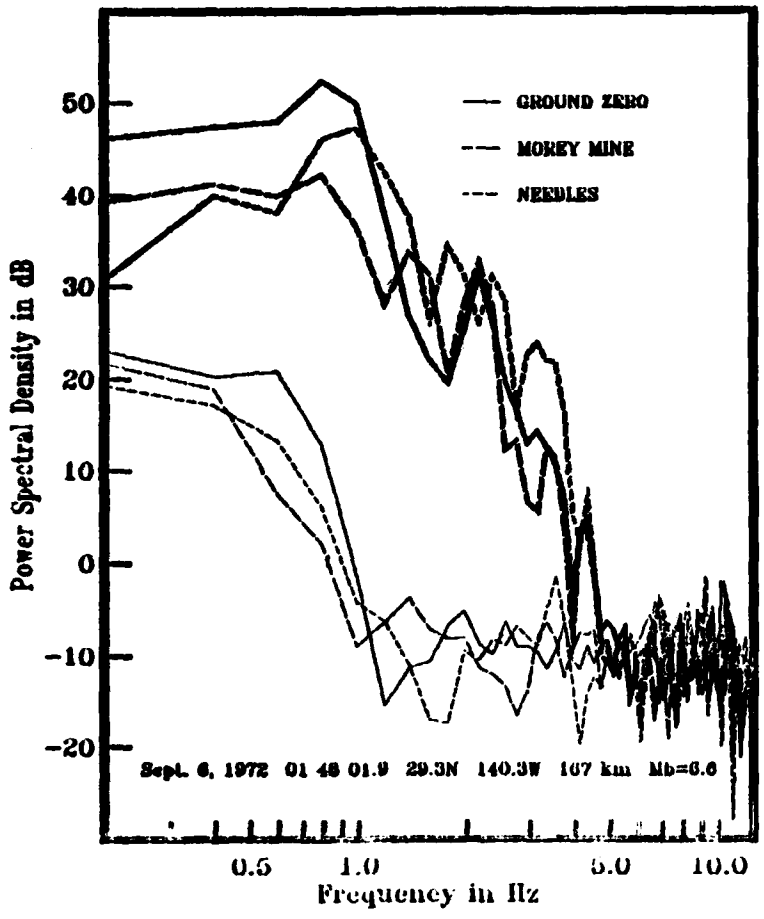
GROUND ZERO
MOREY MINE
NEEDLES
Power Spectral Density in dB
50
40
30
20
10
0
-10
-20
Sept. 6, 1972 01 48 01.9 29.3N 140.3W 107 km Mb=6.6
0.5
1.0
5.0
10.0
Frequency in Hz

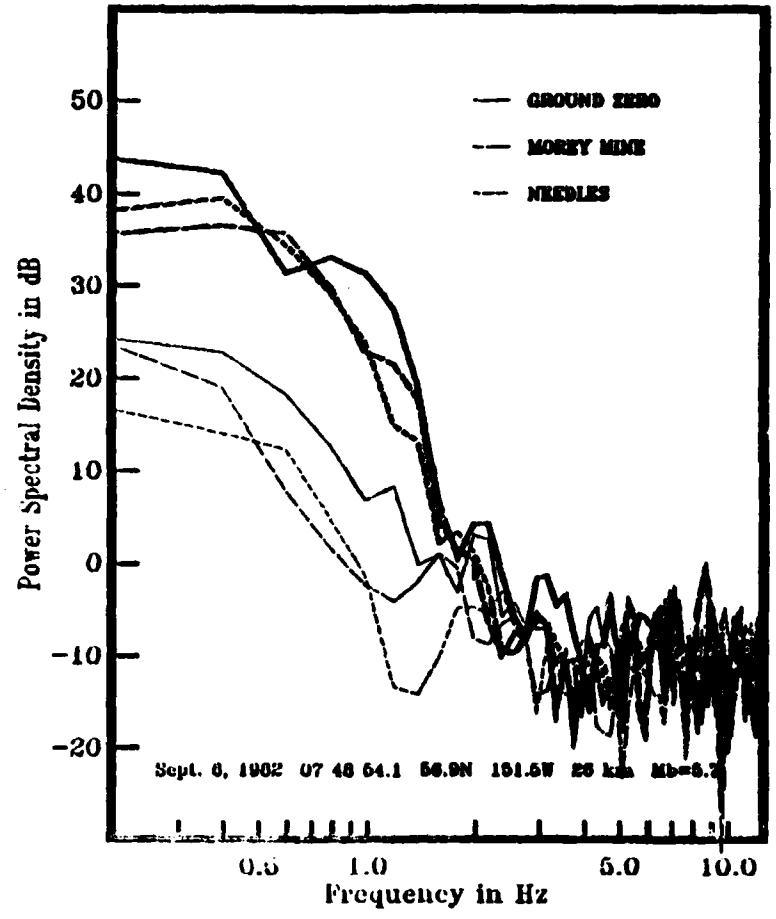
GROUND ZERO
MOREY MINE
NEEDLES
Power Spectral Density in dB
50
40
30
20
10
0
-10
-20
0.5
1.0
5.0
10.0
Frequency in Hz

Figure 3.

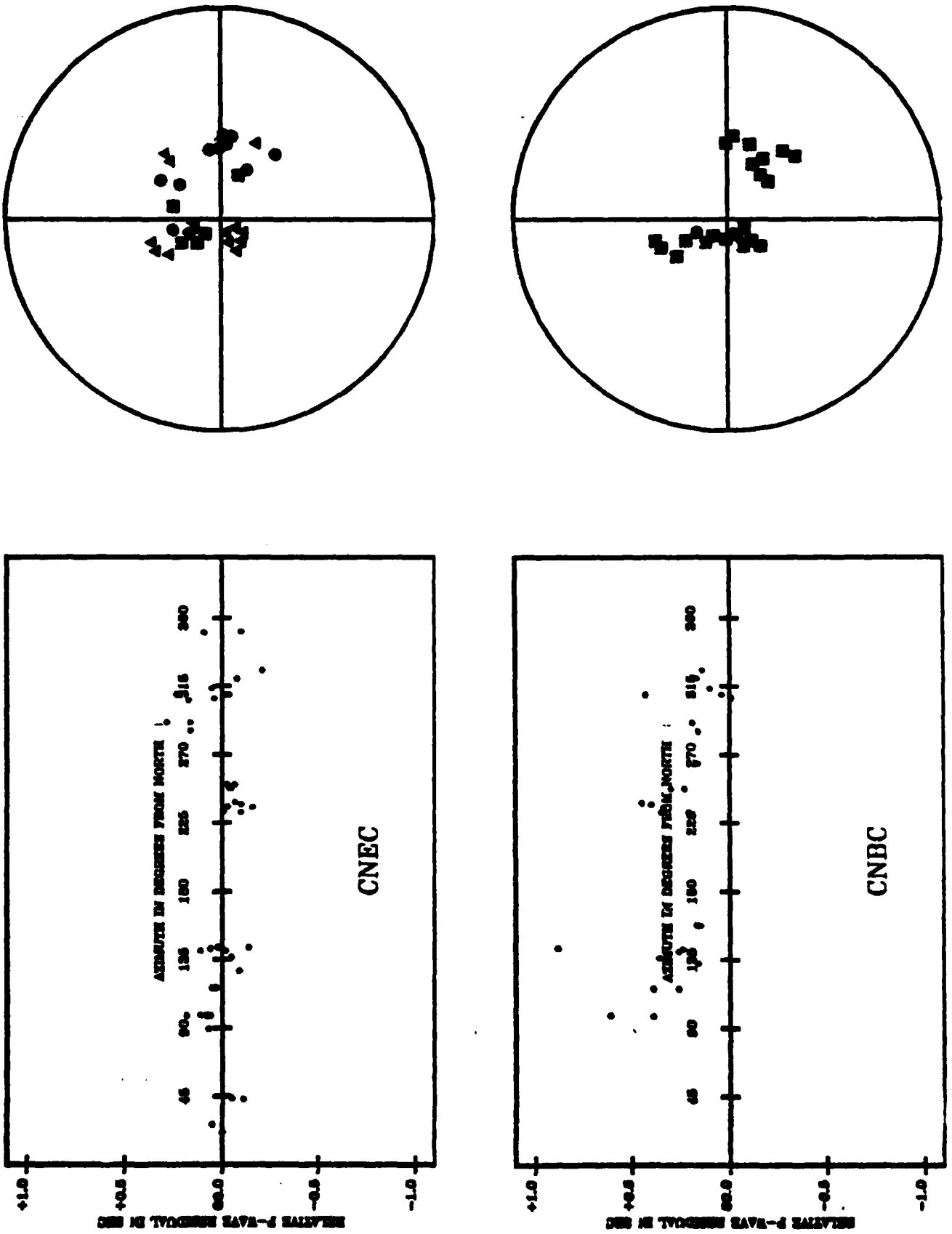

Figure 4a.

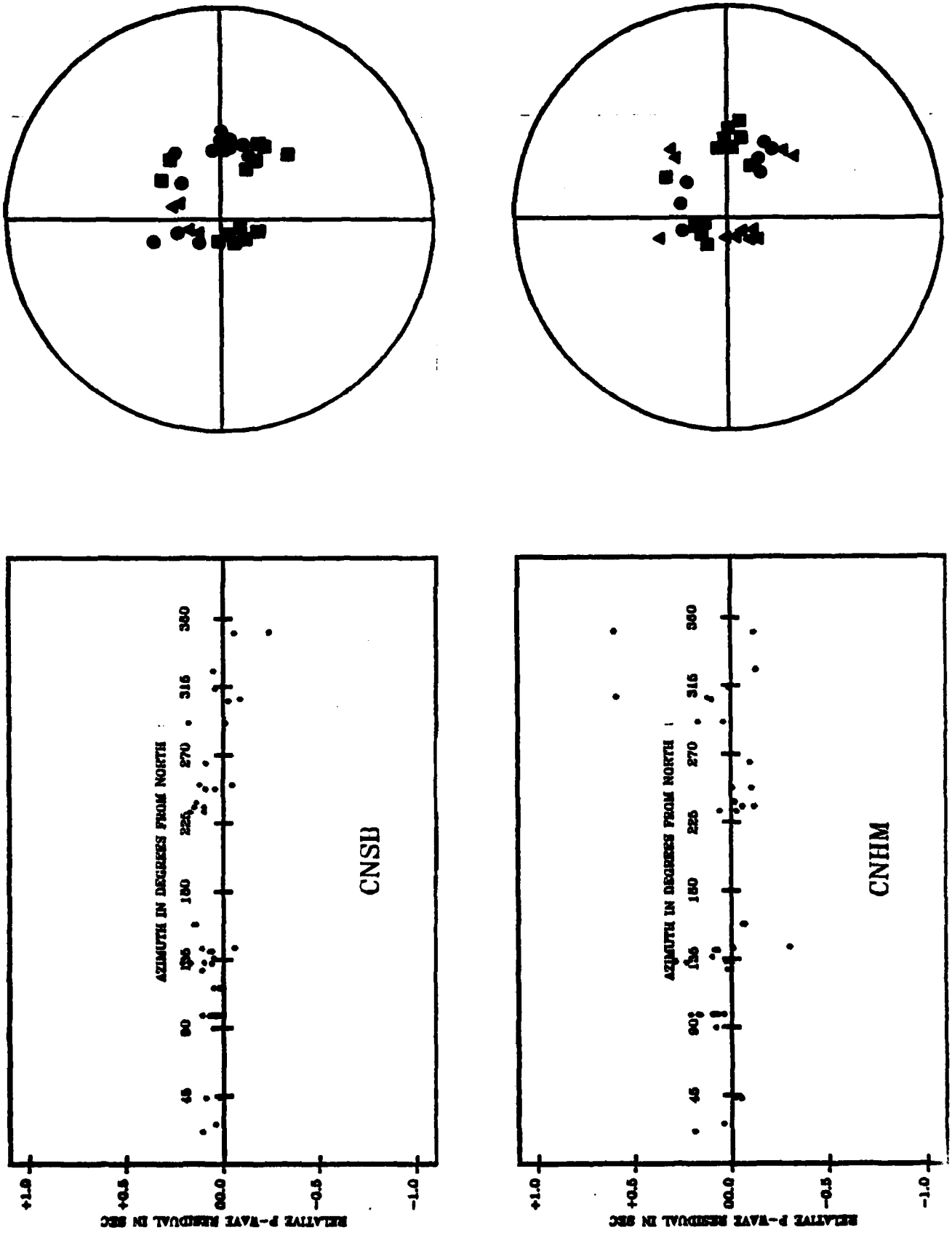
CNSB
CNHM
AZIMUTH IN DEGREES FROM NORTH
RELATIVE P-WAVE RESIDUAL IN SEC
+1.0
+0.5
0.0
-0.5
-1.0
45
90
135
180
225
270
315
360

Figure 4b.

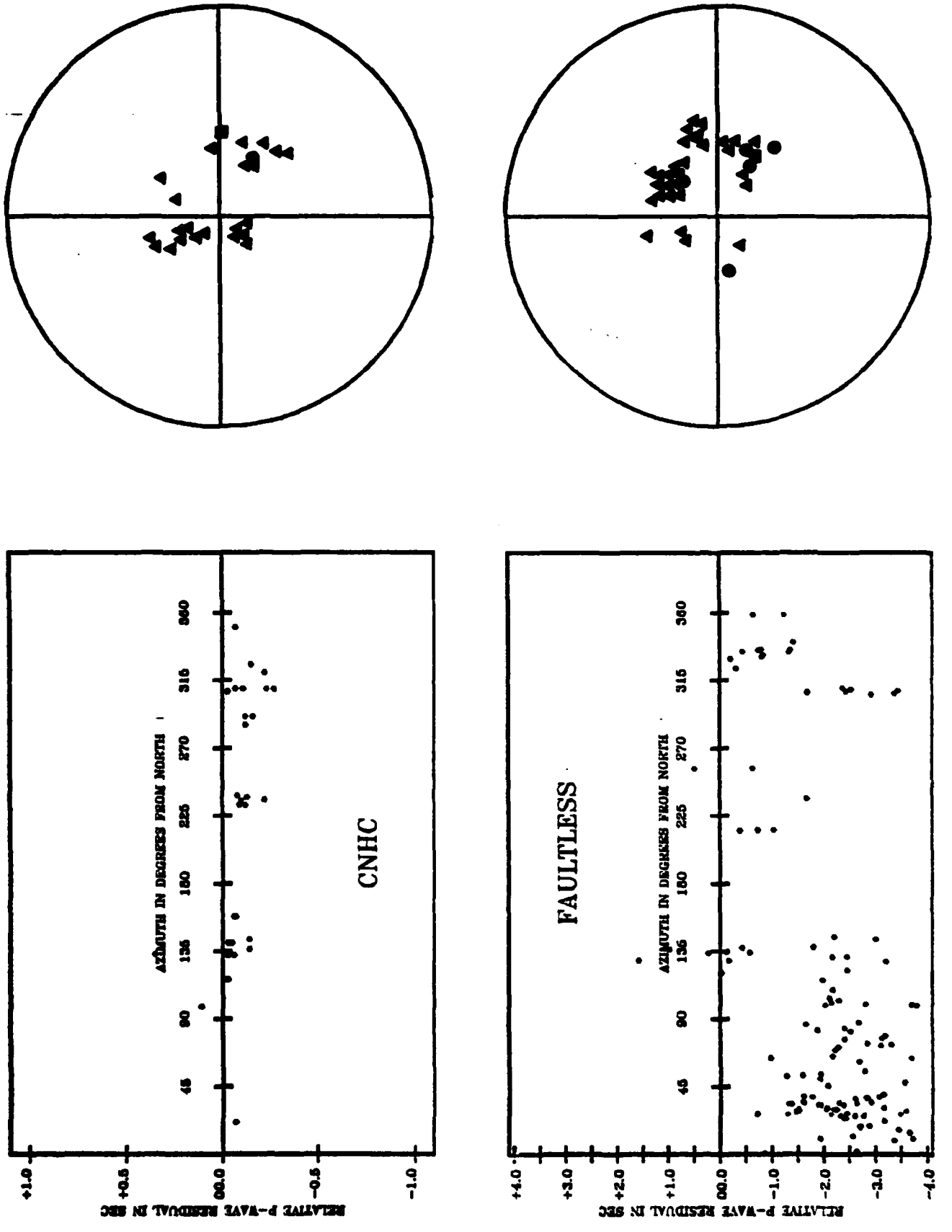
CNHC
FAULTLESS
AZIMUTH IN DEGREES FROM NORTH
RELATIVE P-WAVE RESIDUAL IN SEC

Figure 4c.

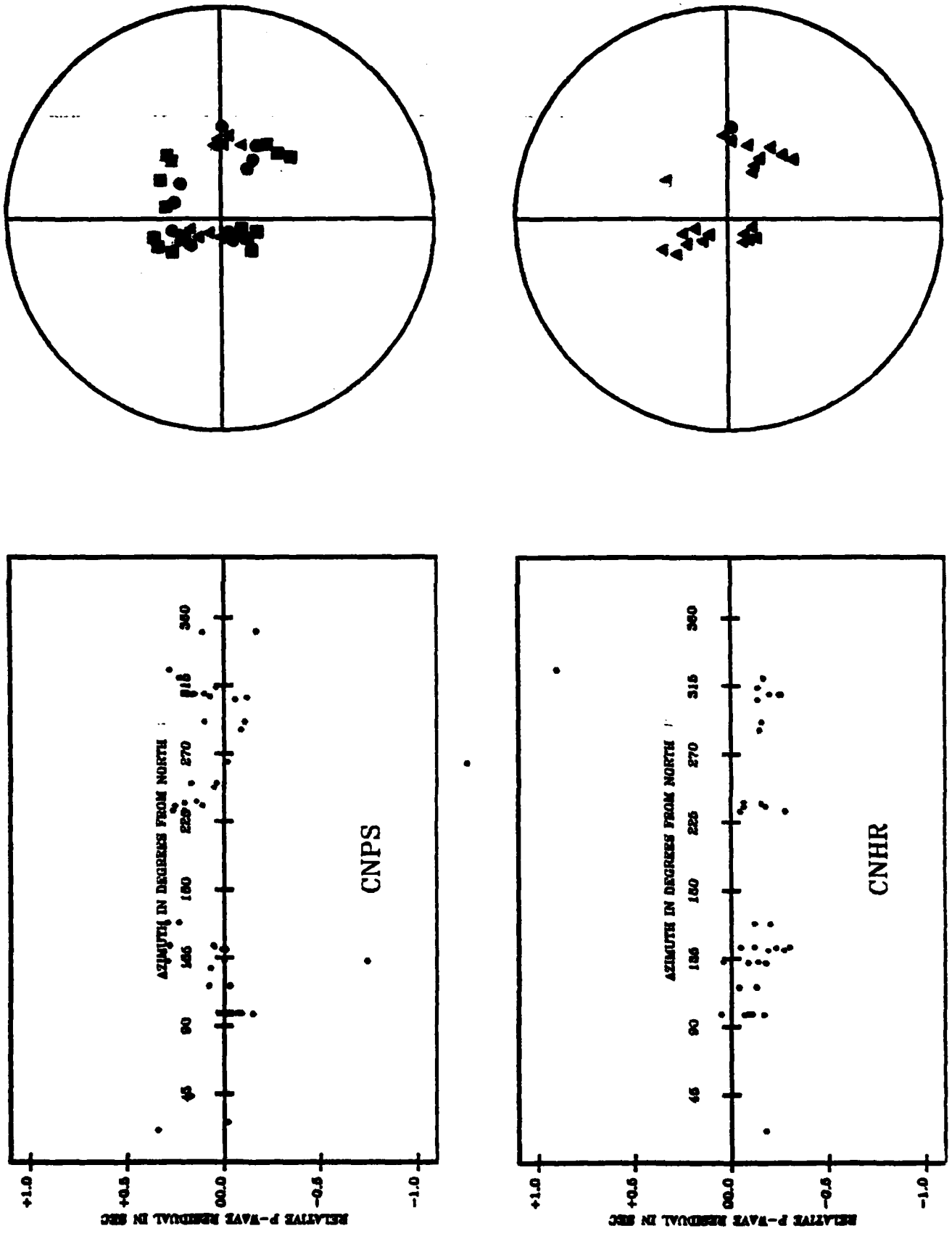
CNPS
CNHR
AZIMUTH IN DEGREES FROM NORTH
RELATIVE P-WAVE RESIDUAL IN SEC
+1.0
+0.5
0.0
-0.5
-1.0
45
90
135
180
225
270
315
360

Figure 4d.

SYSTEMATIC CHANGE OF FOCAL MECHANISM WITH DEPTH IN THE WESTERN GREAT BASIN

Ute R. Vetter and Alan S. Ryall

Seismological Laboratory
University of Nevada
Reno, NV 89557-0018

ABSTRACT

For most areas in the western Great Basin focal mechanisms show a consistent pattern of primarily strike-slip motion for shallow events and oblique or normal slip for deeper events. However, orientation of the axis of least principal stress (*T-axis*) is different for different areas: NW-SE for western Nevada and the Mono Lake region, and NE-SW for the Mammoth Lakes area. Along the remainder of the Sierra Nevada frontal fault zone, T-axes show both orientations.

In general the change in mechanism with depth is interpreted as the result of increasing overburden pressure, resulting in rotation of the maximum compressive stress (*P-axis*) from horizontal at depths less than about 6 km to vertical at depths greater than about 9 km. The absence of normal-slip events at depths greater than 10 km in one area (Mono-Excelsior-Luning zone) may be explained by a larger horizontal compressive stress compared with areas that do have normal faulting at such depths. In some areas conjugate right- and left-lateral shear on nearly vertical fractures may be associated with the formation of clusters of magma-filled dikes at shallow depths.

Assuming strike-slip faulting to be characteristic of earthquakes with depth less than 6 km and normal faulting for events deeper than 10 km, extrapolation of measured shear stress in the upper few kilometers of the crust provides a rough estimate of the maximum and minimum principal stress as a function of depth. At about 3 km depth we find that S_1 and S_3 are both horizontal, with values of about 104 and 55 MPa, respectively. At depth of 20 km S_1 is vertical and equal to the overburden pressure, about 530 MPa; S_3 is horizontal and about 260-300 MPa.

INTRODUCTION

The Great Basin is a region of active crustal spreading characterized by a system of horsts and grabens, thin crust, high heat flow, low P_n velocity and relatively low gravity (Stewart, 1971; Thompson and Burke, 1974). Structurally the region is interpreted in terms of block-faulting, with alternating grabens and horsts forming a series of parallel valleys and mountain ranges. In some cases valleys and mountain ranges are formed respectively by the downslope and upslope parts of tilted blocks (Stewart, 1978). Tectonically the province has been formed by lithospheric extension in an almost east-west direction, possibly involving the brittle fragmentation of a crustal slab above a plastically extending lower medium (Stewart, 1971). Different tectonic theories to explain the regional extension are given by Stewart (1978).

The Great Basin is characterized by a complex system of faults. The main fault segments have north to northeast trends; northwest trends are also observed, primarily in the southwest part of the region. Both normal and strike-slip motion are associated with Basin and Range faulting. The Walker Lane, a northwest-trending zone in western Nevada, is characterized by right-lateral strike slip and represents a boundary between NNW-trending structures to the west and NNE trends to the east (Slemmons *et al.*, 1979; Bell and Slemmons, 1979). On the other hand the Olinghouse, Midas, Carson and Mono-Excelsior lineaments in western Nevada have northeast trend and left-lateral strike slip (Sanders and Slemmons, 1979). The proportion of strike-slip to dip-slip motion appears to increase from north to south in the region.

Published focal mechanisms for the western Great Basin and adjacent Sierra Nevada show normal-, oblique- and strike-slip movement (*e.g.*,Ryall and Malone, 1971; Koizumi *et al.*, 1973; Smith and Lindh, 1978; VanWormer and Ryall, 1980). Fault-plane solutions for earthquakes in the western Great Basin indicate

a generally consistent trend (about N60°W) for the axis of minimum compressive stress (*T-axis*), in agreement with regional lithospheric extension in the same direction (Ryall and Malone, 1971). However, for events in the Sierra Nevada frontal fault zone (VanWormer and Ryall, 1980; Cramer and Toppozada, 1980) T-axis trends of E-W to ENE-WSW are reported.

Fault-plane solutions for recent earthquakes in northwestern and western Nevada show primarily dip- or oblique-slip movement, and surface ruptures show the same type of displacements. The Fairview Peak earthquake in 1954, for example, had a focal mechanism with a strong strike-slip component, agreeing very well with geodetic measurements (Romney, 1957; Slemmons, 1957). The mechanism for the Rainbow Mountain-Stillwater earthquakes of 1954 also had a component of strike-slip motion, although the surface ruptures showed primarily vertical slip (Tocher, 1955; 1956). Gumper and Scholz (1971) presented fault-plane solutions for seven large earthquakes plus two composite solutions for small events, all located in the western Great Basin along a zone from the northern Owens Valley to Winnemucca. They found predominantly normal faulting, frequently with a right-lateral strike-slip component. They interpreted the latter as a superposition of right-lateral shear stress on a general E-W crustal extension. As an exception, the authors found primarily left-lateral movement on an E-W strike-slip fault for a composite mechanism in the Excelsior Mountains, and interpreted this as a transform fault between two extensional zones. However, Ryall and Priestley (1975) reinterpreted that mechanism as oblique slip on a fault striking NE.

According to Ryall and Malone (1971) focal mechanisms in the Fairview Peak-Dixie Valley rupture zone are consistent with an interpretation of simple block faulting, with faults of different orientation having the same slip direction and a consistent orientation of about N60°W for the T-axis. However, Ryall and

Vetter (1982) found that strike-slip and oblique-slip mechanisms tended to occur at different depths in the Fairview Peak-Dixie Valley zone, and attributed the change to a rotation of the maximum compressive stress (*P-axis*) related to increasing overburden pressure with depth. Gumper and Scholz (1971) and VanWormer and Ryall (1980) found that mechanisms south of the Fairview Peak zone, in Cedar Valley, Mina and Mono Valley were consistent with right-oblique slip on faults striking NNW and dipping east.

In studies of the 1980 Mammoth Lakes, California, earthquake sequence different mechanisms for the same events have been determined from local and teleseismic data. For the larger events of this sequence, fault-plane solutions determined from recordings in the California-Nevada region (Cramer and Toppozada, 1980; Ryall and Ryall, 1981a) indicate primarily strike-slip motion (left-lateral on N-S striking planes or right-lateral on E-W planes). However, long-period data collected at *teleseismic distance for the same events* require oblique slip on moderately-dipping faults (Given *et al.*, 1982) or a non-double couple component in the moment tensors (Barker and Langston, 1982; B. Julian, written communication). Given *et al.* suggest that this discrepancy may be due either to distortion of the radiation pattern by structure or to source complexity. In the latter case, they hypothesize that the short-period arrivals may reflect failure (strike-slip) of an asperity which, when broken, allows the regional strain to be relieved with the mechanism (oblique slip) determined from the long-period data. Observations of surface ruptures for the 1980 Mammoth Lakes earthquakes indicate primarily dip slip or oblique slip (Taylor and Bryant, 1980; Clark *et al.*, 1982). Savage and Clark (1982) suggest reinflation of a magma chamber at mid-crustal depth in Long Valley caldera to explain both observed surface deformation associated with the 1980 sequence, as well as the earthquakes themselves.

A detailed discussion of the oblique-slip earthquakes is given by Zoback and Zoback (1980a,b) in which they attribute the mechanism to slip on pre-existing faults that have orientation different from that dictated by the present stress regime. In their study of fault patterns in north-central Nevada they hypothesize a stesss field in the form $S_V = S_{NNE} > S_{WNW}$ (*i.e.*, $S_1 = S_2 > S_3$), so that local variations in the magnitude of S_V and S_{NNE} determine which type of faulting occurs: if $S_V > S_{NNE}$ the slip is normal or oblique, but if $S_{NNE} > S_V$ the movement is strike-slip. Zoback and Zoback also suggest that the Sierra Nevada marks a transition from primarily strike-slip motion along the San Andreas fault system to primarily extensional tectonics of the Basin and Range province. In this transition zone they postulate that the extensional tectonics and high heat flow of the Great Basin extend 50-100 km into the Sierra.

A number of authors (*e.g.*, Wallace, 1979) have suggested that faulting in the Basin and Range province is listric, with a detachment surface at 15-20 km depth (maximum depth of earthquakes in this region) separating the brittle upper crust from a ductile lower crust. However, at this depth movement would take place through very weak earthquakes or the beginning of aseismic creep, and it would be difficult to find seismic evdence for such a detachment surface.

In a previous report (Ryall and Vetter, 1982) we noted that focal mechanisms for earthquakes in the Fairview Peak-Dixie Valley rupture zone in north-central Nevada were consistent with NW-SE extension, as reported by a number of previous authors. However, there appeared to be a correlation between the ratio of dip-slip to strike-slip motion and increasing focal depth, such that shallow earthquakes were primarily strike-slip and normal faulting predominated at greater depth. This is similar to an observation by Klein *et al.* (1977) that mechanisms for a 1972 Reykjanes Peninsula swarm were strike-slip for depth less than 3 km and mostly normal for greater depth.

In the present investigation we have determined focal mechanism for a large number of earthquakes in the western Great Basin and eastern Sierra Nevada, and find that the correlation between depth and mechanism that we observed for the Fairview Peak-Dixie Valley zone generally obtains for the entire western Great Basin-eastern Sierra Nevada region.

ANALYSIS AND RESULTS

The data base for this study consisted mainly of recordings from the Nevada seismic network of 30-50 stations (depending on time of occurrence of a particular event). Supplementary data were obtained from stations operated in California by the University of California, the US Geological Survey and California Institute of Technology, as well as stations in Utah operated by the University of Utah.

Most of the hypocenters for these events were calculated with the HYPO71 algorithm of Lee and Lahr (1975); a few were determined using a program written by W. A. Peppin for Nevada network data. In both cases a simple crustal model was used consisting of a 28 km-thick layer with P-wave velocity 6.0 km/sec over a half-space with velocity 7.9 km/sec. A north-trending record section for earthquakes near Mammoth Lakes, California, indicated that a better crustal model for the western Great Basin would include an intermediate layer with P-wave velocity 6.7 km/sec in the depth range 22-28 km. Work by other authors (Thompson and Burke, 1974; Prodehl, 1979; Priestley *et al.*, 1982) indicates that the crust is thicker and more complex along the Sierra Nevada-Great Basin boundary zone. However, because most of our observations were made either in the Great Basin, where intermediate phases do not appear as first arrivals for the range of event depths in this study, or at P_n distances in California, the simple crustal model was assumed to be adequate for both hypocenter

determination and analysis of first-motion patterns.

Most of the events used in this investigation had location quality of "A" or "B", usually corresponding to standard error (i.e., precision of the calculation) of less than a kilometer in depth and permitting a comparison between events at different depth ranges in the same area. However, it should be kept in mind that absolute accuracy of the hypocenter calculation is a function of the model used, and the depth of all events in a given area could vary systematically by as much as a few kilometers.

Depth Distribution

Figure 1 shows frequency of earthquake occurrence as a function of depth for all A and B quality events recorded and located since 1970. The plot indicates maximum occurrence in the 7-10 km range, with an approximately symmetric decrease for smaller and larger depth. Plotting the same earthquakes as a function of both depth and magnitude (Figure 2) shows that the small earthquakes scatter over a greater depth range than the stronger events. Thus, earthquakes with $M_L \geq 2.0$ are strongly concentrated in the 5-10 km depth range, while most events with $M_L < 2.0$ occur at depths of 5-15 km and are concentrated in the 10-15 km range.

Focal Mechanisms

More than 130 fault-plane solutions were determined for this study, and 108 were sufficiently well-determined for a detailed comparison of mechanism as a function of event location and depth. All of the solutions were for individual events and are based on at least 15 first-motion observations; in many cases 20-30 points were available. Nearly all of the mechanisms are consistent with extensional (normal or oblique slip) or strike-slip faulting, primarily on planes striking in a northerly direction but ranging from NW-SE to NE-SW. In agree-

ment with our previous observations for the Fairview Peak-Dixie Valley zone (Ryall and Vetter, 1982) we find indications for a systematic change in focal mechanism with depth for nearly all parts of the region studied. The general picture shows strike- and oblique-slip faulting to be characteristic in the uppermost 8-10 km in the crust, and oblique and normal faulting to predominate below this depth. In the following sections mechanisms will be discussed for four separate areas within the western Great Basin: Mammoth Lakes, western Nevada, the Mono-Excelsior-Luning zone, and the Sierra Nevada-Great Basin boundary zone exclusive of the Mammoth Lakes area.

Mammoth Lakes area. The most significant activity in terms of number and size of events has occurred in the Mammoth Lakes area since 1978; in general the Mammoth Lakes earthquakes also had good station coverage and azimuthal distribution of observations. We studied 44 earthquakes in this area, 36 of which had *A* or *B* quality hypocenter determinations. In Figures 3 and 4 we show fault-plane solutions for 34 of these events, separated respectively into groups with focal depth less than or greater than 9 km. All the plots on these and successive figures are lower-hemisphere, equal-angle projections, with compression quadrants shaded. A list of the locations and mechanism parameters for these events is given in Table 1. The earthquakes in the figures are numbered with increasing depth, in accordance with the listing in Table 1.

Figure 3 indicates that for Mammoth Lakes events with depth less than about 9 km focal mechanisms are rather consistent and predominantly strike-slip. The picture is less clear for greater depth (Figure 4), but most solutions show a relatively larger component of normal slip and some events show almost pure normal faulting. There are some strike-slip events at depth greater than 9 km, but almost no shallow shocks were found with predominant dip-slip motion. One event at shallow depth even had a reverse-faulting component (#26). The

change in mechanism with depth is illustrated by Figure 5, which shows two earthquakes that occurred at the same epicenter, nine minutes apart in time and with a difference of 6 km in depth. The first, with a strike-slip mechanism, was the shallower event (depth 8.2 km); the second, deeper (14.2 km) shock, had a strong normal-slip component.

Western Nevada. Figures 6 and 7 show fault-plane solutions in western Nevada, respectively for depths less than and greater than 9 km; hypocenter coordinates and parameters of the fault-plane solutions for these earthquakes are listed in Table 2. Events in the Mono basin, Excelsior Mountains and Luning area will be shown in another figure and discussed separately. Because the western Nevada sample contained only events with smaller magnitude than the Mammoth Lakes sample, station coverage for the former was not as complete as for the latter, and focal depths were not as well constrained. Only the best solutions are shown on Figures 6 and 7, but many of them had *C*-quality locations. In general, focal depths in this part of the western Great Basin are somewhat larger than those near Mammoth Lakes, most having depth greater than 9 km. Similar to Mammoth Lakes, there is a tendency for the larger shocks to cluster in a small depth range: Moderate earthquakes in the Fairview Peak area were concentrated in the 9-14 km depth range, and the deepest shocks (depths around 20 km) were located near Schurz, north of Walker Lake. Most of these deep events were too small for detailed fault-plane solutions; of the few events that were well-enough constrained (Figure 7) all had oblique or normal slip.

In spite of somewhat less constraint on focal depth, a comparison of fault-plane solutions for western Nevada gives similar results as for the Mammoth Lakes events. The mean depth for strike-slip events is 7 km, while for oblique- and normal-slip events it is 12 and 13 km, respectively.

Mono-Excelsior-Luning zone. The most active part of the Mono basin-

Excelsior Mountains-Luning zone is just east of Mono Lake near the California-Nevada border. Migration of earthquakes along this zone in 1980 was interpreted by C. Lide (personal communication) as a propagating strain pulse, suggesting structural continuity at depth. As a result events in this zone are shown separately on Figure 8 for the Mono basin and on Figure 9 for the Excelsior Mountains and Luning area. Locations and parameters of the fault-plane solutions are listed for these events in Table 3; most of the hypocenter determinations were of quality *A* or *B*.

Within this zone the tendency for normal faulting is weak. There were no normal-slip events at all in the Mono basin (Figure 8) and southern Excelsior Mountains (area SW of Mina on Figure 9), despite the fact that more than a third of the events had depth in the 9-12 km range. There is, however, a trend to normal faulting for shocks in the northern Excelsior Mountains and Luning area (areas W and N of Mina on Figure 9). In agreement with other areas, the mean depth of strike-slip events is about 5 km and for oblique-slip events it is 9.5 km.

Sierra Nevada-Great Basin boundary zone. Earthquakes for the Sierra Nevada-Great Basin boundary zone (SNGBZ) exclusive of the Mammoth Lakes area are shown on Figure 10. Strictly speaking, only those earthquakes on the left side of the figure are in the Sierran frontal fault zone; the others are in the westernmost Great Basin but have characteristics similar to events along the Sierra. Two of the mechanisms (#4, #8) were also shown on Figures 6 and 7.

Of the 15 mechanisms shown on Figure 10 and listed in Table 4, only two are for events shallower than 9 km. In general a tendency toward normal faulting dominates this picture, which is in agreement with the greater depth of the earthquakes. However, focal mechanisms for this zone are not as consistent as in the other regions shown on previous figures: T-axes for the SNGBZ show both the NW-SE trend of the western Nevada region and the NE-SW trend of the Mam-

moth sequence.

DISCUSSION

Two main observations result from this investigation. First, moderate-to-strong earthquakes in the western Great Basin and eastern Sierra Nevada tend to cluster in the 5-10 km depth range. Second, focal mechanisms for events in this region are characterized by a change from strike- to oblique- to normal-slip with depth.

The tendence for larger events to cluster in a limited depth range may be explained by recent papers of Sibson (1982) and Meissner and Strehlau (1982), dealing with the maximum depth of intraplate earthquakes as a function of the transition from brittle to ductile behavior of rocks, which in turn is a function of the temperature regime of the region. Based on results of laboratory experiments on quartz-bearing rocks with water content ranging from dry to saturated they concluded that maximum shear stress will occur at a characteristic depth for a particular region. Comparison of frequency-depth plots for well-recorded intraplate earthquakes gave good agreement with the calculations: the most frequent and largest earthquakes tended to occur at a depth corresponding to the calculated maximum stress. In our case the concentration of earthquakes between 8 and 12 km depth is in accordance with predicted maximum shear stress for an extensional regime, wet quartz rheology (water-saturated), and heat-flow between 1.7 and 2.0 HFU (Meissner and Strehlau, 1982). The occurrence of only small (M_L < 2) earthquakes at depth greater than about 12 km suggests that shear resistance at such depths is weak in this region.

In the previous sections we have shown that much of the western Great Basin is characterized by a systematic change in focal mechanisms -- from strike-slip for shallow earthquakes to oblique- or normal-slip at depths greater than about 9-10 km. As illustrated by Figure 11, this appears to be due pri-

marily to a change in plunge of the P-axis. Thus, for the Mammoth Lakes sequence Figure 11(a) shows that T-axes are close to horizontal and have rather consistent NE-SW trend. On the other hand, while the *trend* of the P-axes is also constant, the *plunge* changes – from almost horizontal for shallow earthquakes to almost vertical at larger depth. Similar relationships can be seen on Figures 11(b) and 11(c) for the western Great Basin and the SNGBZ, respectively.

This observed change in mechanism with depth appears to occur gradually. The mean depth for all of the purely strike-slip earthquakes is about 5 km, for oblique- but mostly strike-slip motion it is 6.2 km, for events with about equal amounts of horizontal and vertical movement it is 10.6 km, and for earthquakes with mostly normal slip it is 13.6 km. While there are a few mechanisms on Figures 3-10 that do not fit this pattern, the fact that average behavior with depth is systematic for a number of regions strongly suggests that the type of faulting for a given earthquake is determined by regional extension plus a depth-dependent stress component, and not by pre-existing faults (Zoback and Zoback, 1980a, b) or simple block faulting (Ryall and Malone, 1971).

Estimation of Principal Stresses. These observations can be used to estimate the magnitude of the principal stresses with depth. For pure strike-slip movement the maximum compressive stress is horizontal and the intermediate stress is vertical, while for normal faulting this situation is reversed. Our results indicate that the first stress pattern exists at depths less than 5-6 km, and that the second pattern dominates at depths greater than 9-10 km. For intermediate depths oblique mechanisms indicate a gradual rotation of the P-axis from horizontal to vertical, i.e., an exchange of the maximum and intermediate stress axes. The stress field suggested by Zoback and Zoback (1980a, b), with $S_1 \approx S_2 \gg S_3$ and S_1 vertical, seems to be characteristic for events with depth greater than 9 km, where we find normal or normal-oblique solutions. At depths

less than about 6 km the predominance of strike-slip solutions indicates that $S_1 > S_2 > S_3$, with S_2 vertical. For most of the solutions S_3 is close to horizontal; however, the average trend of this axis is NE-SW for events in the Mammoth Lakes area, NW-SE for the western Great Basin, and scattered for the SNGBZ north of Mammoth Lakes (Figures 11a, b and c, respectively). In the following paragraphs we consider pore pressure P_0, overburden pressure S_V and differential stress $(S_1 - S_3)$ to roughly estimate the principal stresses S_1 and S_3. Results of this estimation are plotted on Figure 12.

The overburden pressure S_V is determined by the equation $S_V = \rho g z$ where the average density $\rho \approx 2.7 gm/cm^3$ for crustal rocks. Pore pressure P_0 is assumed to be hydrostatic. Numerous authors have suggested that pore pressure is hydrostatic to at least mid-crustal depths (*e.g.*, Brace 1971; 1972). Raleigh, *et al.* (1976) found pore pressure of 17 MPa at 2 km depth in Colorado, a value that is approximately equal to hydrostatic. As shown by Zoback and Zoback (1980a, b) the least principle stress S_3 must be greater than the pore pressure.

Measurements of maximum shear stress $\tau_{max} = (S_1 - S_3)/2$ in the upper few kilometers of the crust have been interpreted by Haimson (1977), McGarr and Gay (1978), Zoback and Roller (1979) and Zoback *et al.* (1977). These papers indicated that shear stress increases approximately linearly with depth, and is lower in soft rock than in hard rock. For the latter McGarr (1980) gives the relationship

$$\tau_{max} = 5.67 + 6.37\, z, \qquad (1)$$

where τ_{max} is in MPa and z is in km. An estimate of the shear stress at 10 km depth in north-central Nevada by Zoback and Zoback (1980a) was 64-77 MPa, assuming hydrostatic pore pressure. This is in good agreement with equation (1), which gives 69.4 MPa for a depth of 10 km. Figure 12 shows the differential

stress ($S_1 - S_3$), taken as twice the value of τ_{max} in equation (1).

As noted above, mechanisms for depths larger than about 9 km are normal or oblique. From Jaeger and Cook (1969) frictional sliding on preexisting faults will occur at a critical ratio of the effective stresses,

$$\frac{\sigma_1}{\sigma_3} = [(\mu^2 + 1)^{1/2} + \mu]^2, \tag{2}$$

where μ is the coefficient of friction. From data presented by Byerlee (1978) μ is about 0.65 at a depth of 10 km and 0.63 at 20 km. Using the relationship $\sigma = S - P_0$, between effective stress σ, total stress S and pore pressure P_0, equation (2) leads to

$$S_3 = \frac{(S_1 - P_0)}{[(\mu^2 + 1)^{1/2} + \mu]^2} - P_0, \tag{3}$$

where in the case of normal faulting $S_1 = S_V$, the overburden pressure. Equation (3) gives S_3 = 147 MPa at depth 10 km and 298 MPa at 20 km. These values for the least principle stress are shown as points (1) and (2) on Figure 12.

Somewhat lower estimates of S_3 can be obtained as follows: Noting that the average depth for oblique mechanisms is 10.6 km, we set the overburden pressure S_V equal to the maximum horizontal stress S_H at that depth (point 3 on Figure 12, 281 MPa). Then from equation (1) with $S_1 = S_V$ we can estimate S_3 at 10.6 and 20 km, respectively, as 134 and 263 MPa (points 4 and 5 on Figure 12).

For depths less than about 5 km fault-plane solutions for the western Great Basin are almost pure strike-slip. For this type of faulting, according to Sibson (1974) the overburden pressure S_V will be the intermediate stress S_2 and

$$S_V = S_2 = \frac{S_3 + S_1}{2}. \tag{4}$$

If we assume that pure strike-slip faulting occurs at 3 km depth, then equations

(1) and (4) give values for S_1 and S_3, respectively, of 104 and 55 MPa. In this case S_1 is the maximum horizontal stress S_H and a line connecting points (3) and (7) on Figure 12 gives a rough estimate of the increase in this stress with depth.

Variation in T-axis trends. As shown by Figure 11, T-axes (axes of minimum compressive stress S_3) for this study have maximum plunge of 40° but in most cases are almost horizontal. The mean value of the T-axis plunge for all of the events studied is about 8°, with no systematic change with depth. Trend of the T-axes is NW-SE for events in the western Great Basin and Mono basin, with a peak in the direction N50-70°W (Figure 3a).

For the Mammoth Lakes area T-axes trend NE-SW, with only 5 of 44 events failing to show this trend (Figure 3B). Earthquakes along the rest of the Sierra Nevada frontal fault system show a range of trends from NW-SE to NE-SW, indicating that this zone is a region of transition between two stress systems. This pattern generally agrees with the finding of VanWormer and Ryall (1980) that mechanisms along the Sierran frontal fault zone are different than those in central Nevada. Our findings also agree with those of Zoback and Zoback (1980b) for the northern Sierra Nevada, but not for the southern Sierra where they found NW-SE T-axes. Hill (1982) suggested that the NE-SW T-axis for the Mammoth Lakes sequence represents an anomaly in a region of otherwise NW-SE extension, but our results suggest that the NE-SW orientation is not unusual for this zone.

Variations in fault dip. A decrease in dip of the fault plane with increasing focal depth is indicated by the parameters listed in Tables 1-4. Thus, for the shallow event shown on Figure 5 both the fault and auxiliary planes have a dip of 80° or more, while the two planes for the deeper event have dips of 64° and 38°. Regardless of which plane is taken to be the fault plane, this would signify a

change from steep dip near the surface to smaller dip at larger depth. Similarly, the mean dip of the fault and auxiliary planes for all the events we studied is about 80°-90° for earthquakes shallower than 6 km, 70°-75° for depths of 6-9 km, and 55°-60° for events deeper than 9 km. This shows a decrease in fault-plane dip by about 25° from the surface to about 15 km depth. While this observation might by itself be taken as support for listric faulting, other evidence indicates that this is not the case. Nowhere, for example, have we seen the very shallow dips that would be associated with a detachment surface at midcrustal depth. Further, the sense of motion -- strike-slip at shallow depth, oblique or normal at larger depth -- is not appropriate for listric faulting.

Lithospheric extension by faulting and magma injection. While our observations are not consistent with listric faulting, they do support the idea that lithospheric extension in the western Great Basin involves both tectonic and magmatic processes. To illustrate this we recall that most of the deeper earthquakes in this area are associated with oblique-to-normal slip along faults parallel to the Sierra Nevada frontal fault system, striking N-S to NW-SE (Figure 4). However, the shallower events have strike-slip mechanisms -- right-lateral slip on planes striking about N75°W and/or left-lateral slip on planes striking about N10°E (Figure 3). In an earlier paper Hill (1977) pointed out that shallow strike-slip events are commonly observed in volcanic regions, and proposed a model to explain this pattern in which conjugate shear failures on nearly vertical fractures accompany the formation of magma-filled dikes. Comparison of his model with focal mechanisms for the Mammoth Lakes sequence suggests that strike-slip events in *and around* Long Valley caldera may be associated with the formation of clusters of NW-trending fissures or magma-filled dikes (Figure 13; Ryall and Ryall, 1983). At greater depth, extension would take place mainly through faulting instead of dike formation. The existence of magma at shallow

depth, at least within the caldera, is indicated by teleseismic P-delays (Steeples and Iyer, 1976), possible reflections on an explosion profile (Hill, 1976), lack of S-waves for paths through the caldera (Ryall and Ryall, 1981b), uplift of the resurgent dome (Savage and Clark, 1982) and spasmodic tremor in a small area near Mammoth Lakes (Ryall and Ryall, 1983).

Such a tectonic/volcanic process would be consistent with an earlier suggestion by Lachenbruch and Sass (1978) that lithospheric extension in the Basin and Range province takes place through a combination of normal faulting and magmatic intrusion of the brittle crust. According to those authors, volcanic centers like Long Valley caldera exist "because they are at places where the lithosphere is pulling apart rapidly, drawing up basalt from below to fill the void." Our observation that a systematic change in focal mechanism with depth is also characteristic of other parts of the western Great Basin suggests that a combination of faulting and magmatic activity may be fairly common for this entire region.

Finally, it should be noted that our analysis was based primarily for earthquakes in the range M_L = 3-5, and does not necessarily apply either to major (M > 7) earthquakes in the region or to microearthquakes with M_L < 3. For the former, field evidence indicates that major oblique- or normal-slip events at mid-crustal depths rupture to the surface to produce range-front faults with the same type of slip. In the case of the strong earthquakes at Mammoth Lakes in 1980, it is possible that strike-slip movement associated with the breaking of a shallow asperity may have triggered a larger oblique-slip event at depth, as suggested by Given *et al* (1982), leading to oblique-slip motion observed at the surface by Taylor and Bryant (1980) and Clark *et al.* (1982). To extend this study we are currently studying smaller (M_L < 3) earthquakes to try and determine whether they behave in the same systematic way as the moderate-sized events.

ACKNOWLEDGEMENT

This research was partly supported by the U. S. Geological Survey under contract 14-08-0001-21248, and partly by the U. S. Department of Energy under contract DE-AS08-82ER12082. The research was also partly supported by the Advanced Research Projects Agency of the Department of Defense and was monitored by the Air Force Office of Scientific Research under Contract No. F49620-83-C-0012.

REFERENCES

Barker, J. S., and Langston, C. A., A teleseismic body wave analysis of the May 1980 Mammoth Lakes, California, earthquakes, *Bull. Seismol. Soc. Am.*, *73*, 1983, in press.

Bell, E. J., and Slemmons, D. B., Recent crustal movements in the central Sierra Nevada-Walker Lane region of California-Nevada: Part II, the Pyramid Lake right-slip fault zone segment of the Walker Lane, *Tectonophysics*, *52*, 571-583, 1979.

Brace, W. F., Resistivity of saturated crustal rocks to 40 km based on laboratory measurements, in *Structure and Physical Properties of the Earth's Crust, Geophys. Monogr. Ser., 10*, ed. J. G. Heacock, 243-255, 1971.

Brace, W. F., Pore pressure in geophysics, in *Flow and Fracture of Rocks, Geophys. Monogr. Ser., vol. 16*, ed. H. C. Heard, 265-273, 1972.

Byerlee, J. D., Friction of rocks, *Pure Appl. Geophys.*, *116*, 615-626,1978.

Clark, M. M., Yount, I. C., Vaughan, P. R., and Zepeda, R. L., *Ruptures associated with the Mammoth Lakes, California, earthquakes of May 1980*, U.S. Geol. Survey, Map 1398, Denver, 1982.

Cramer, C. H., and Toppozada, T. R., A seismological study of the May 1980 and earlier earthquake activity near Mammoth Lakes, California, *Calif. Div. Mines Geol. Spec. Rep., 150*, 91-130, 1980.

Given, J. W., Wallace T. C., and Kanamori, H., Teleseismic analysis of the 1980 Mammoth Lakes earthquake sequence, *Bull. Seismol. Soc. Am., 72*, 1093-1109, 1982.

Gumper, J. C. and Scholz. C., Microseismicity and tectonics of the Nevada seismic zone, *Bull. Seismol. Soc. Am., 61*, 1413-1432, 1971.

Haimson, B. C., Crustal stress in the continental United States as derived from hydrofracturing tests, in *The Earth's Crust, Geophys. Monogr. Ser., 20*, ed. J. G. Heacock, 576-592, 1977.

Hill, D. P., Structure of Long Valley caldera from a seismic refraction experiment, *J. Geophys. Res., 81*, 745-753, 1976.

Hill, D. P., A model for earthquake swarms, *J. Geophys. Res., 82*, 1347-1352, 1977.

Hill, D. P., Contemporary block tectonics: California and Nevada, *J. Geophys. Res., 87*, 5433-5450, 1982.

Jaeger, J. C., and Cook, N. G. W., *Fundamentals in Rock Mechanics*, 515 pp, Chapman and Hall, London, 1969.

Klein, F. W., Einarsson, P., and Wyss, M., The Reykjanes Peninsula, Iceland, earthquake swarm of September 1972 and its tectonic significance, *J. Geophys. Res., 82*, 865-888, 1977.

Koizumi, C. J., Ryall, A., and Priestley, K. F., Evidence for a high-velocity lithospheric plate under northern Nevada, *Bull. Seismol. Soc. Am., 63*, 2135-2144, 1973.

Lachenbruch, A. H., and Sass, J. H., Models of an extending lithosphere and heat flow in the Basin and Range province, *Geol. Soc. Am. Mem.*, *152*, 209-250, 1978.

Lee, W. H. K., and Lahr, J. C., HYPO71 (revised): A computer program for determining hypocenter, magnitude, and first motion pattern of local earthquakes, *U. S. Geol. Surv. Open File Rep. 75-311*, 113 pp, 1975.

McGarr, A., Some constraints on levels of shear stress in the crust from observations and theory, *J. Geophys. Res.*, *85*, 6231-6238.

McGarr, A., and Gay, N. C., State of stress in the earth's crust, *Ann. Rev. Earth Planet. Sci.*, *6*, 405-436, 1978.

Meissner, R., and Strehlau, J., Limits of stresses in continental crusts and their relation to the depth-frequency distribution of shallow earthquakes, *Tectonics*, *1*, 73-89, 1982.

Priestley, K. F., Ryall, A. S., and Fezie, G. S., Crust and upper mantle structure in the northwest Basin and Range province, *Bull. Seismol. Soc. Am.*, *72*, 911-923, 1982.

Prodehl, C., Crustal structure of the western United States, *U. S. Geol. Surv. Prof. Pap.*, *1034*, 74pp, 1979.

Raleigh, C. B., Healy, J. H., and Bredehoeft, J. D., An experiment in earthquake control at Rangely, Colorado, *Science*, *191*, 1230-1237, 1976.

Romney, C., The Dixie Valley-Fairview Peak, Nevada, earthquakes of December 16, 1954: seismic waves, *Bull. Seismol. Soc. Am.*, *47*, 301-320, 1975.

Ryall, A., and Malone, S. D., Earthquake distribution and mecahnism of faulting in the Rainbow Mountain-Dixie Valley-Fairview Peak area, central Nevada, *J. Geophys. Res.*, *76*, 7241-7248.

Ryall, A., and Priestley, K., Seismicity, secular strain, and maximum magnitude in the Excelsior Mountains area, western Nevada and eastern California, *Geol. Soc. Am. Bull.*, *86*, 1585-1592, 1975.

Ryall, A., and Ryall, F., Spatial-temporal variations in seismicity preceding the May, 1980, Mammoth Lakes, California, earthquakes, quakes, *Bull. Seism. Soc. Am.*, *71*, 27-39, 1981a.

Ryall, A. and Ryall, F., Attenuation of P and S waves in a magma chamber in Long Valley caldera, California, *Geophys. Res. Letters*, *8*, 557-560, 1981b.

Ryall, A., and Ryall, F., Spasmodic tremor and possible magma injection in Long Valley caldera, eastern California, *Science*, 1983, in press.

Ryall, A. S., and Vetter, U. R., *Seismicity Related to Geothermal Development in Dixie Valley, Nevada*, Final Rept. on USDOE Contr. DE-AC08-79NV10054, Univ. of Nevada, Reno, 102 pp., 1982.

Sanders, C. O., and Slemmons, D. B., Recent crustal movements in the central Sierra Nevada-Walker Lane region of California-Nevada: Part III, the Olinghouse fault zone, *Tectonophysics*, *52* 585-597, 1979.

Savage, J. C., and Clark, M. M., Magmatic resurgence in Long Valley caldera, California: Possible cause of the 1980 Mammoth Lakes earthquakes, *Science*, *217*, 531-533, 1982.

Scholz, C.H., Barazangi, M., and Sbar, M. L., Late Cenocoic evolution of the Great Basin, western United States, as an ensialic interarc basin, *Geol. Soc. Am. Bull.*, *82*, 2979-2990, 1971.

Sibson, R. H., Frictional constraints on thrust, wrench, and normal faults, *Nature*, *249*, 542-544, 1974.

Sibson, R.H., Fault zone models, heat flow, and the depth distribution of earthquakes in the continental crust of the United States, *Bull. Seismol. Soc. Am.*, *72*, 151-163, 1982.

Slemmons, D. B., Geological effects of the Dixie Valley-Fairview Peak, Nevada, earthquakes of December 16, 1954, *Bull. Seismol. Soc. Am.*, *47*, 353-375, 1957.

Slemmons, D. B., VanWormer, D., Bell, E. J., and Silberman, M. L., Recent crustal movements in the Sierra Nevada-Walker Lane region of California-Nevada: Part I, rate and style of deformation, *Tectonophysics*, *52*, 571-583, 1979.

Smith, R. B., and Lindh, A. G., Fault-plane solutions of the western United States: A compilation, *Geol. Soc. Am. Mem.*, *152*, 107-109, 1978.

Stewart, J. H., Basin and Range structure: A system of horsts and grabens produced by deep-seated extension, *Bull. Geol. Soc. Am.*, *82*, 1019-1044, 1971.

Stewart, J. H., Basin-Range structure in western North America: A review, *Geol. Soc. Am. Mem.*, *152*, 1-31, 1978.

Taylor, G. C., and Bryant, W. A., Surface rupture associated with the Mammoth Lakes earthquakes of 25 and 27 May, 1980, *Calif. Div. Mines Geol. Spec. Pap.*, *150*, 49-67, 1980.

Thompson, G. A., and Burke, D. B., Regional geophysics of the Basin and Range province, *Ann. Rev. Earth Planet. Sci.*, *2*, 213-228, 1974.

Tocher, D., *Seismic velocities and structure in northern California and Nevada*, PhD Thesis, Univ. of California, Berkeley, 1955.

Tocher, D., Movement on the Rainbow Mountain fault, *Bull. Seismol. Soc. Am.* *46*, 10-14, 1956.

VanWormer, J. D., and Ryall, A. S., Sierra Nevada-Great Basin boundary zone: Earthquake hazard related to structure, active tectonic processes, and anomalous patterns of earthquake occurence, *Bull. Seismol. Soc. Am.*, *70*, 1557-1572, 1980.

Wallace, R. E., Earthquakes and the pre-fractured state of the western part of the North American continent, in *Proceed. of the Conf. on Intracontin. Earthquakes*, Sept. 1979, Ohrid, Yugoslavia, 69-81, Skopje, 1979.

Wallace T. C., Lyzenga, G. A., and Given, J. W., A discrepancy between long- and short-period fault mechanisms of earthquakes near the Long Valley caldera, (abstr.), *Earthquake Notes, 53*, 46, 1982.

Zoback, M. D., Healy, J. H., and Roller, J. C., Preliminary stress measurements in central California using the hydraulic fracturing technique, *Pure Appl. Geophys., 115*, 135-152, 1977.

Zoback, M. D., and Roller, J. C., Magnitude of shear stress on the San Andreas Fault: Implication from a stress measurement profile at shallow depth, *Science, 206*, 445-447, 1979.

Zoback, M. L., and Zoback, M. D., Faulting patterns in north-central Nevada and strength of the crust, *J. Geophys. Res., 85*, 275-284, 1980a.

Zoback, M. L., and Zoback M. D., State of stress in the conterminous United States, *J. Geophys. Res., 85*, 6113-6156, 1980b.

Table 1. Mammoth Lakes Area: Location and fault-plane solution parameters for events shown on Figures 3 and 4, listed in order of increasing depth. (a)--Number; (b)--Date; (c)--Time GMT; (d)--Latitude, ^{o}N; (e)--Longitude, ^{o}W; (f)--Focal Depth, km; (g)--M_L; (h)--Q; (i)--Strike and Dip of Plane A; (j)--Strike and Dip of Plane B.

(a)	(b)	(c)	(d)	(e)	(f)	(g)	(h)	(i)	(j)
1	1982 8 5	1538	37.616	118.898	2.8	3.4	B	N 36 E 79^{o}	N 60 W 60^{o}
2	1980 5 27	1901	37.592	118.781	3.9	4.8	B	N 36 E 90^{o}	N 54 W 90^{o}
3	1981 9 30	1153	37.569	118.689	4.0	5.2	B	N 20 E 79^{o}	N 71 W 82^{o}
4	1980 6 11	440	37.539	118.881	4.3	4.6	B	N 31 E 90^{o}	N 59 W 73^{o}
5	1980 6 4	2100	37.600	118.913	4.5	3.3	A	N 17 E 80^{o}	N 71 W 85^{o}
6	1980 6 1	1727	37.571	118.769	4.9	3.9	A	N 22 E 90^{o}	N 66 W 86^{o}
7	1981 9 30	1433	37.609	118.863	5.7	3.8	B	N 16 E 70^{o}	N 75 W 82^{o}
8	1981 11 13	350	37.618	118.930	6.0	3.3	B	N 06 W 66^{o}	N 76 W 50^{o}
9	1980 5 25	1633	37.618	118.809	6.5	6.1	B	N 05 E 86^{o}	N 86 W 86^{o}
10	1982 5 8	357	37.632	118.942	6.9	4.1	A	N 04 E 68^{o}	N 76 W 68^{o}
11	1980 5 31	058	37.488	118.846	7.1	4.5	B	N 10 E 73^{o}	N 88 W 66^{o}
12	1981 10 9	1101	37.629	118.865	7.6	4.1	B	N 18 E 80^{o}	N 73 W 90^{o}
13	1981 10 2	737	37.625	118.853	7.7	4.2	B	N 14 E 90^{o}	N 76 W 90^{o}
14	1981 11 13	307	37.619	118.930	7.8	4.2	B	N 08 W 62^{o}	N 76 W 50^{o}
15	1981 11 13	300	37.619	118.931	7.9	4.0	B	N 16 E 86^{o}	N 74 W 70^{o}
16	1981 8 9	1552	37.618	118.920	8.2	3.7	B	N 15 E 80^{o}	N 54 W 80^{o}
17	1981 8 24	452	37.608	118.885	8.4	4.0	B	N 11 W 56^{o}	N 77 W 58^{o}
18	1981 9 30	1427	37.623	118.859	8.6	3.1	B	N 04 W 64^{o}	N 76 W 60^{o}

Table 1. Continued

(a)	(b)			(c)	(d)	(e)	(f)	(g)	(h)	(i)		(j)	
19	1981	8	22	2054	37.614	118.886	8.8	3.8	B	N 22 W	51°	N 40 W	40°
20	1981	8	6	2231	37.517	118.832	8.9	3.8	B	N 60 E	78°	N 26 W	70°
21	1980	6	1	2230	37.619	118.882	9.2	3.7	B	N 65 W	46°	N 72 W	44°
22	1981	3	25	401	37.530	118.864	9.6	3.7	B	N 11 E	60°	N 43 W	45°
23	1981	9	25	648	37.525	118.871	9.9	3.9	B	N 46 E	50°	N 32 W	75°
24	1980	6	23	632	37.564	118.829	10.6	5.5	B	N 05 E	64°	N 90 W	82°
25	1980	6	13	2323	37.491	118.812	10.9	4.0	B	N 78 E	75°	N 22 W	56°
26	1980	6	14	735	37.498	118.833	11.0	3.5	B	N 65 E	37°	N 63 W	66°
27	1981	3	5	528	37.524	118.880	11.1	3.9	B	N 10 E	47°	N 37 W	54°
28	1980	6	23	516	37.580	118.834	11.1	5.6	B	N S	80°	N 21 W	60°
29	1980	6	27	129	37.575	118.839	11.1	3.7	B	N 21 W	40°	N 21 W	50°
30	1980	6	8	2322	37.473	118.833	11.4	4.3	B	N 10 E	50°	N 19 E	40°
31	1981	9	17	1236	37.540	118.855	12.4	3.5	B	N S	60°	N 80 W	70°
32	1980	5	26	1224	37.526	118.874	12.4	5.1	B	N 19 W	50°	N 69 W	50°
33	1981	11	5	330	37.537	118.812	13.7	3.5	B	N 34 W	63°	N 82 W	38°
34	1981	8	9	1601	37.619	118.919	14.2	4.3	B	N 03 E	64°	N 50 W	38°

Table 2. Western Nevada (Figures 6, 7). Column headings same as Table 1.

(a)	(b)			(c)	(d)	(e)	(f)	(g)	(h)	(i)			(j)		
1	1979	7	26	923	39.601	118.070	3.4	3.1	C	N 58 W	70°		N 32 E	85°	
2	1982	7	6	210	37.655	114.992	4.0	4.7	B	N 20 W	90°		N 70 E	90°	
3	1978	1	13	339	39.388	117.588	5.0	4.5	C	N S	50°		N 70 E	70°	
4	1978	9	5	2229	39.041	118.169	5.4	3.4	C	N 62 W	75°		N 32 E	70°	
5	1980	4	8	013	39.517	119.160	6.9	4.9	C	N 24 W	90°		N 66 E	70°	
6	1980	5	19	1806	39.159	118.071	8.4	3.2	C	N 24 E	24°		N 30 E	65°	
7	1979	7	26	1038	39.592	118.074	8.5	4.2	C	N 56 W	60°		N 34 E	90°	
8	1979	7	26	1052	39.601	118.114	8.7	3.2	C	N 74 W	60°		N 24 E	74°	
9	1981	3	10	1719	39.027	118.201	9.2	3.3		N 26 E	54°		N 63 E	43°	
10	1980	7	28	1322	39.187	118.086	9.2	3.1	B	N 05 E	49°		N 24 E	42°	
11	1977	8	8	451	37.568	117.756	9.3	4.2	C	N 15 E	50°		N 51 E	42°	
12	1982	3	5	1009	38.308	118.702	10.5	2.6	C	N 05 E	54°		N 10 E	36°	
13	1980	9	20	2114	38.839	118.810	10.6	3.8		N 13 E	54°		N 45 E	42°	
14	1980	9	26	607	39.471	118.133	11.8	3.2	B	N 66 W	62°		N 45 E	54°	
15	1978	2	15	925	39.552	118.442	12.0	4.0		N 11 E	60°		N 64 E	42°	
16	1977	12	31	343	38.899	117.984	12.4	3.1	C	N 18 E	50°		N 31 E	40°	
17	1981	11	11	1615	38.399	117.050	12.7	2.8		N 68 W	80°		N 12 E	60°	
18	1981	4	29	1155	39.297	119.780	12.8	4.2		N 19 W	44°		N 04 E	49°	
19	1982	5	15	1333	38.753	118.795	13.0	2.5	C	N 35 W	60°		N 48 E	78°	

(a)	(b)	(c)	(d)	(e)	(f)	(g)	(h)	(i)	(j)
20	1977 8 4	1120	38.873	118.003	14.7	3.0	C	N 20 E 52°	N 45 E 40°
21	1980 9 21	449	38.829	118.846	15.0	3.2		N 03 E 49°	N 47 E 50°
22	1979 11 6	525	39.084	118.334	15.3	3.0	C	N S 46°	N 32 E 48°
23	1976 1 28	617	38.617	118.942	16.1	4.1	C	N 38 W 74°	N 61 E 59°
24	1982 3 28	1413	39.702	118.437	16.3			N 04 E 50°	N 43 E 46°
25	1980 4 11	1928	39.439	119.177	17.0	2.6	D	N 25 E 60°	N 50 E 33°
26	1982 1 15	203	38.817	118.818	17.6	1.9		N 15 W 55°	N 14 E 38°
27	1980 11 25	1844	39.063	118.942	18.0	2.2		N 45 W 70°	N 56 E 60°
28	1980 11 25	1955	39.043	118.932	20.0	2.5		N 35 W 60°	N 62 E 69°
29	1980 9 19	1852	38.810	118.839	25.0	2.4		N S 50°	N 60 E 60°

Table 3. Mono - Excelsior - Luning Zone (Figures 8, 9). Column headings same as Table 1.

(a)	(b)			(c)	(d)	(e)	(f)	(g)	(h)	(i)			(j)		
1	1982	4	25	251	38.036	118.578	2.0	2.8	B	N 74 W	90°		N 16 E	90°	
2	1981	7	13	1637	38.004	118.734	2.9	3.6	B	N 23 W	90°		N 67 E	90°	
3	1981	1	1	1822	38.051	118.567	3.7	4.1	A	N S	90°		N 86 E	70°	
4	1982	4	30	1933	38.175	118.337	3.8	3.6	B	N 26 W	90°		N 64 E	90°	
5	1980	9	21	1515	38.049	118.574	5.3	4.0	A	N 46 W	78°		N 42 E	80°	
6	1982	5	28	326	38.036	118.579	6.2	3.3	A	N 12 W	75°		N 70 E	60°	
7	1980	11	11	1033	38.034	118.571	6.2	4.3	A	N 15 W	60°		N 89 E	64°	
8	1981	4	28	2254	38.038	118.566	6.5	4.6	A	N 12 W	90°		N 78 E	90°	
9	1980	12	28	2258	38.164	118.362	7.0	4.8	B	N 28 W	70°		N 80 E	49°	
10	1981	4	18	035	38.040	118.572	7.7	3.6	A	N 45 W	63°		N 39 E	88°	
11	1981	8	18	016	38.043	118.578	7.7	2.7	A	N 28 W	80°		N 60 E	80°	
12	1981	9	7	436	38.065	118.590	8.4	5.3	B	N 16 W	90°		N 74 E	80°	
13	1980	12	19	1657	38.467	118.399	8.9	4.0	B	N 08 W	80°		N 86 E	70°	
14	1976	1	11	444	38.442	118.323	9.0	3.3	B	N 37 W	88°		N 49 E	48°	
15	1980	9	7	647	38.062	118.589	9.6	5.2	B	N 33 W	73°		N 59 E	80°	
16	1982	5	21	848	38.469	118.155	9.6	3.4	B	N 36 W	84°		N 57 E	48°	
17	1981	9	12	1812	38.067	118.579	9.8	4.4	A	N 12 W	60°		N 79 E	87°	
18	1981	5	7	102	37.926	118.527	9.8	4.6	B	N 16 W	50°		N 60 E	72°	
19	1981	5	7	218	37.929	118.522	9.9	4.0	B	N 10 W	52°		N 66 E	74°	

(a)	(b)			(c)	(d)	(e)	(f)	(g)	(h)	(i)			(j)		
20	1982	1	28	2259	38.580	118.178	9.9	3.5	B	N 90 W	70°		N 08 E	70°	
21	1982	1	28	2330	38.570	118.174	9.9	3.0		N 30 E	43°		N 54 E	49°	
22	1982	1	10	950	38.364	118.274	10.1	2.0	B	N 01 E	62°		N 61 E	45°	
23	1981	12	19	2056	38.581	118.239	10.3	4.7	A	N 22 E	47°		N 28 E	42°	
24	1982	3	28	037	38.479	118.437	10.4	2.2	B	N 36 W	46°		N 71 E	69°	
25	1982	1	29	1838	38.566	118.185	10.5	3.1		N 03 E	50°		N 62 E	62°	
26	1982	5	29	034	38.571	118.193	10.6	2.0	B	N 05 W	33°		N 37 E	64°	
27	1980	9	7	1158	38.063	118.581	11.1	4.0	B	N 15 W	60°		N 67 E	78°	
28	1981	6	20	1427	38.152	118.267	11.7	3.0	B	N 12 W	61°		N 59 E	60°	
29	1981	1	10	1757	38.172	118.369	12.1	2.8	B	N 34 W	78°		N 49 E	61°	
30	1980	4	30	724	38.465	118.397	13.7	3.9	B	N 09 W	70°		N 68 E	60°	

Table 4. Sierra Nevada - Great Basin Boundary Zone (Figure 10). Column headings same as Table 1.

(a)	(b)			(c)	(d)	(e)	(f)	(g)	(h)	(i)			(j)		
1	1980	11	28	1821	39.245	120.496	1.5	5.2	C	N	52	W	80°	N 39	E 80°
2	1982	1	24	1648	37.393	117.920	6.1	2.8		N	28	W	70°	N 66	E 80°
3	1982	5	28	459	39.714	120.530	9.1	2.3	C	N	26	E	65°	N 83	E 40°
4	1977	8	8	451	37.568	117.756	9.3	4.2	C	N	15	E	50°	N 51	E 42°
5	1982	5	9	1919	38.318	119.061	9.7	1.9	B	N	25	W	65°	N 03	W 27°
6	1982	1	24	1543	37.397	117.910	10.1	4.6	B	N	26	W	50°	N 04	W 44°
7	1981	11	18	1615	37.465	119.413	10.1	4.2	C	N	24	W	75°	N 58	E 66°
8	1982	3	5	1009	38.308	118.702	10.5	2.6	C	N		S	54°	N 10	E 36°
9	1980	12	8	1729	38.702	119.452	13.1	2.8		N	55	W	49°	N 06	W 51°
10	1982	1	5	326	39.889	120.673	14.4	3.8		N	54	W	48°	N 41	W 42°
11	1980	12	8	1656	38.692	119.471	15.0	3.7		N	60	W	85°	N 25	E 45°
12	1981	6	11	1414	39.589	122.333	15.1	3.2	B	N	37	W	56°	N 80	E 58°
13	1982	5	13	1039	38.400	119.348	16.3	2.4	B	N	43	W	60°	N 48	E 90°
14	1980	8	15	425	39.533	120.337	17.2	3.0	B	N	69	W	60°	N 02	E 60°
15	1980	11	28	1711	39.261	120.479	18.9	3.5		N	30	W	50°	N 40	E 60°

FIGURE CAPTIONS

Figure 1. Earthquake frequency as a function of focal depth, for events with *A* and *B* quality hypocentral determination in the western Great Basin and eastern Sierra Nevada, 1970-1981. N -- number of earthquakes.

Figure 2. Earthquake frequency (percent) as a function of depth. (a) -- Magnitude ML greater than 2; (b) -- ML less than 2. Only *A* and *B* quality events are shown.

Figure 3. Fault-plane solutions for earthquakes with depth less than 9 km in the Mammoth Lakes area, eastern California. (Lower-hemisphere, equal-angle projection, shaded areas are compressions, numbers correspond to Table 1).

Figure 4. Fault-plane solutions for earthquakes with depth greater than 9 km in the Mammoth Lakes area, eastern California. Numbers correspond to Table 1.

Figure 5. Fault-plane solutions for two Mammoth Lakes events that occured on Aug. 9, 1981 at the same epicentral location. Time (GMT), coordinates, depths (D), magnitudes (M), and quality (B) are given. Closed circles -- compression, open circles -- dilatation, T -- T axis, P -- P axis.

Figure 6. Fault-plane solutions for earthquakes with depth less than 9 km in the western Great Basin. Numbers correspond to Table 2.

Figure 7. Fault-plane solutions for earthquakes with depth greater than 9 km in the western Great Basin. Numbers correspond to Table 2.

Figure 8. Fault-plane solutions for earthquakes east of Mono Lake at the California-Nevada border. Numbers correspond to Table 3.

Figure 9. Fault-plane solutions for earthquakes in the Excelsior Mountains and Luning area of western Nevada. Numbers correspond to Table 3.

Figure 10. Fault-plane solutions for earthquakes in the Sierra Nevada-Great Basin boundary zone. Numbers correspond to Table 4.

Figure 11. Lower-hemisphere equal-angle projection showing P-axes (solid circles) and T-axes (open circles). (a) -- Mammoth Lakes area; (b) -- western Nevada and Mono- Excelsior-Luning zone; (c) – Sierra Nevada-Great Basin boundary zone.

Figure 12. Estimated principal stresses as a function of depth. P_0 – hydrostatic pore pressure, $S_1 - S_3$ -- twice the maximum shear stress measured for hard rocks and extrapolated downwards, $S_h = S_3$ -- smallest horizontal principal stress, S_V – overburden pressure, S_H -- greatest horizontal principal stress. Shaded area shows range of S_3. Points with numbers are described in the text.

Figure 13. Model to explain strike-slip faulting for shallow Mammoth lakes earthquakes. Top left – rose diagram showing orientation of T axes, top right -- rose diagram showing strike of the two fault planes, bottom – model with vertical fissures (dikes) forming together with conjugate right- and left-lateral shears on planes shown.

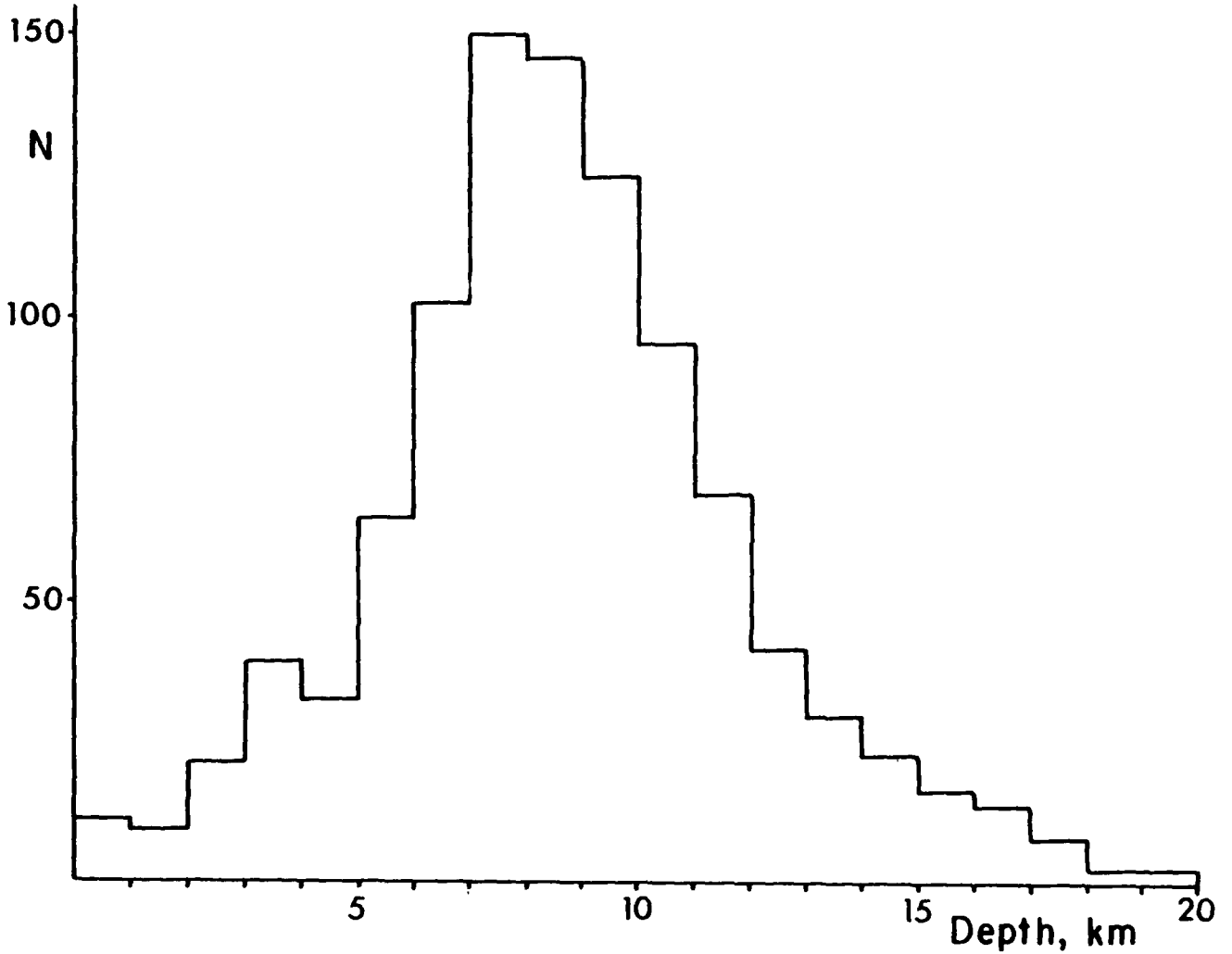

Figure 1

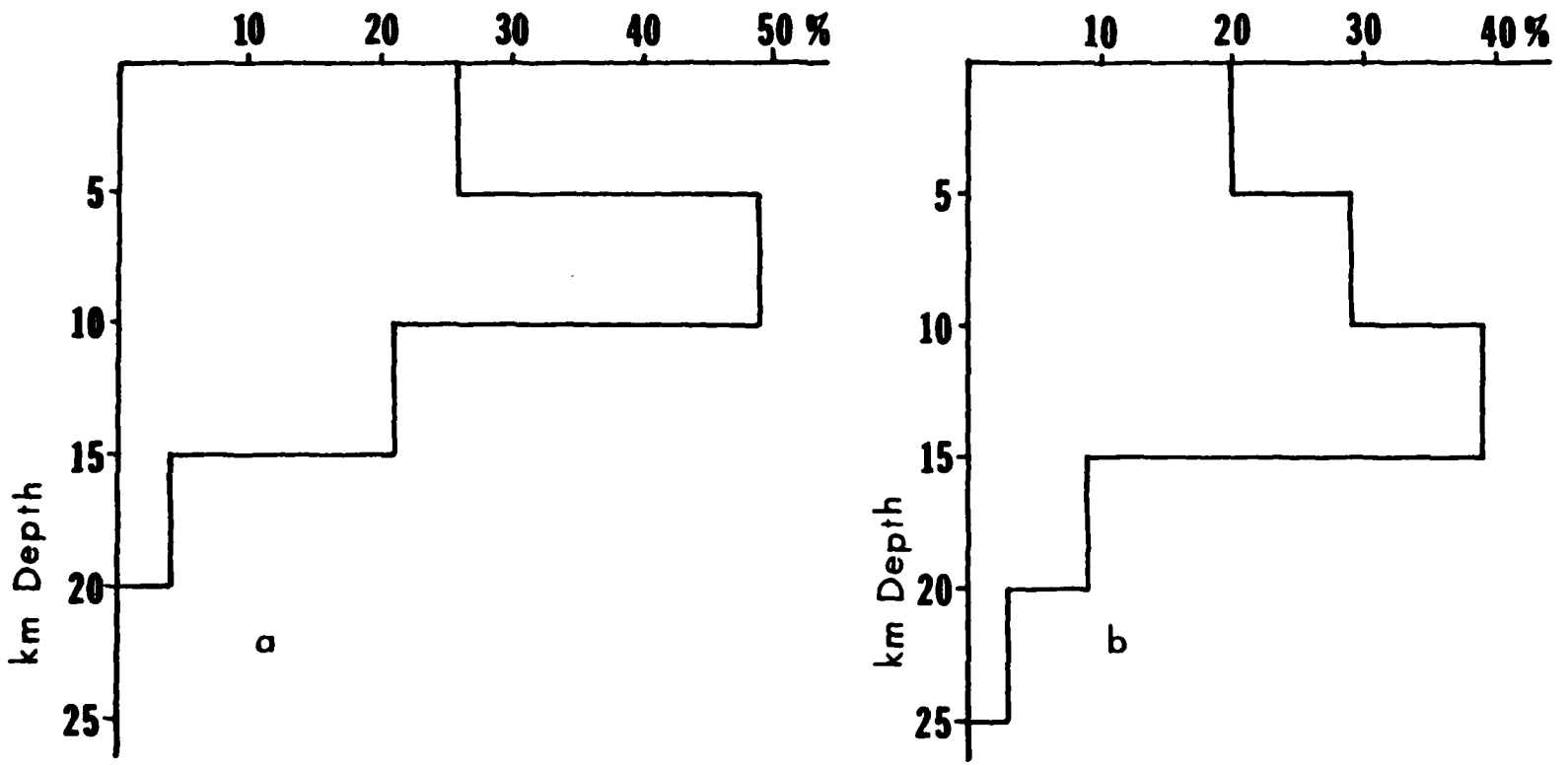
10
20
30
40
50 %
5
10
15
20
25
km Depth
a
10
20
30
40 %
5
10
15
20
25
km Depth
b

Figure 2

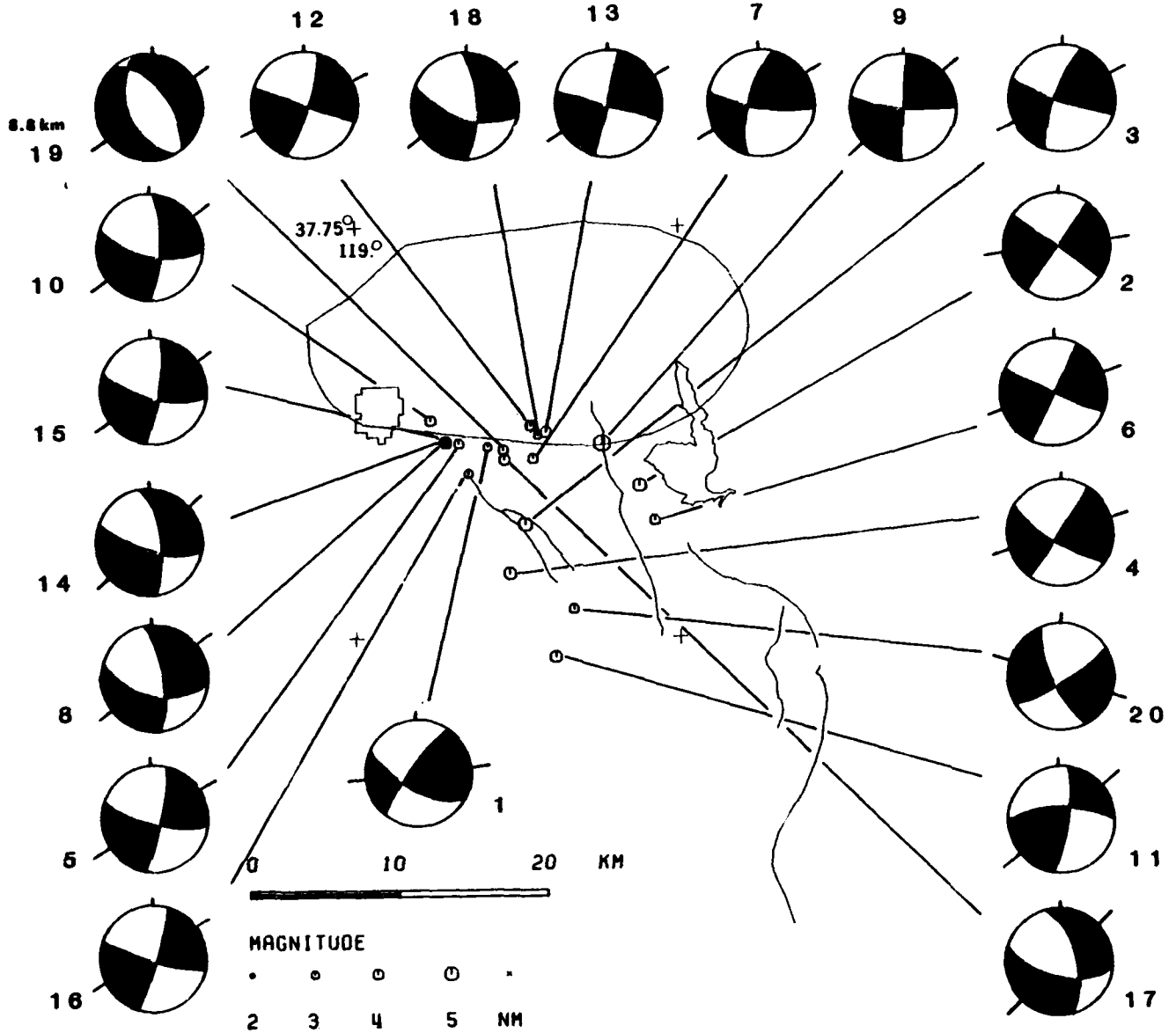
12
18
13
7
9
8.8 km
19
3
10
2
37.75°
119°
15
6
14
4
8
20
1
5
11
0
10
20
KM
MAGNITUDE
2
3
4
5
NM
16
17

Figure 3

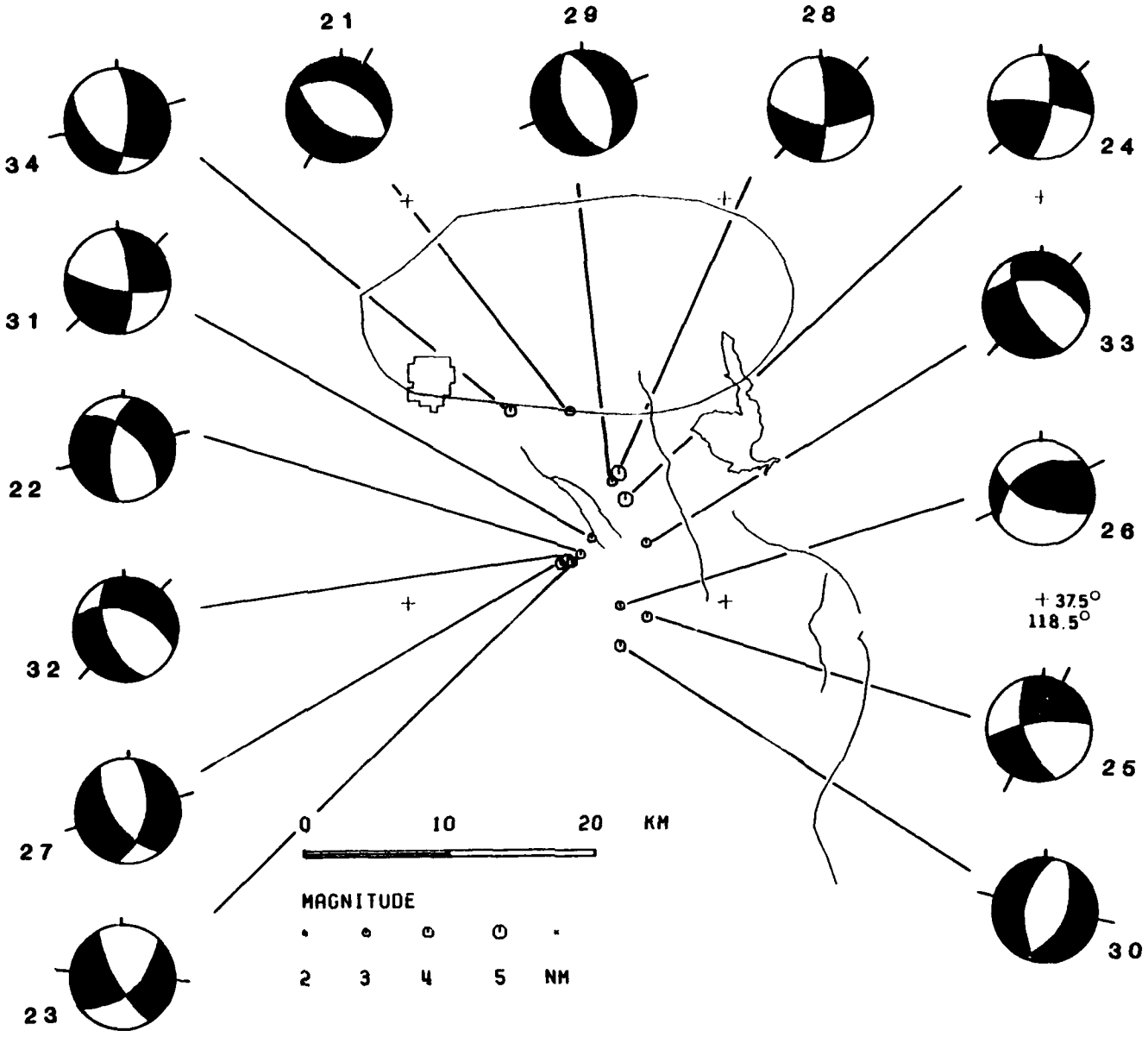
21
29
28
34
24
31
33
22
26
37.5°
118.5°
32
25
27
0
10
20
KM
MAGNITUDE
2
3
4
5
NM
23
30

Figure 4

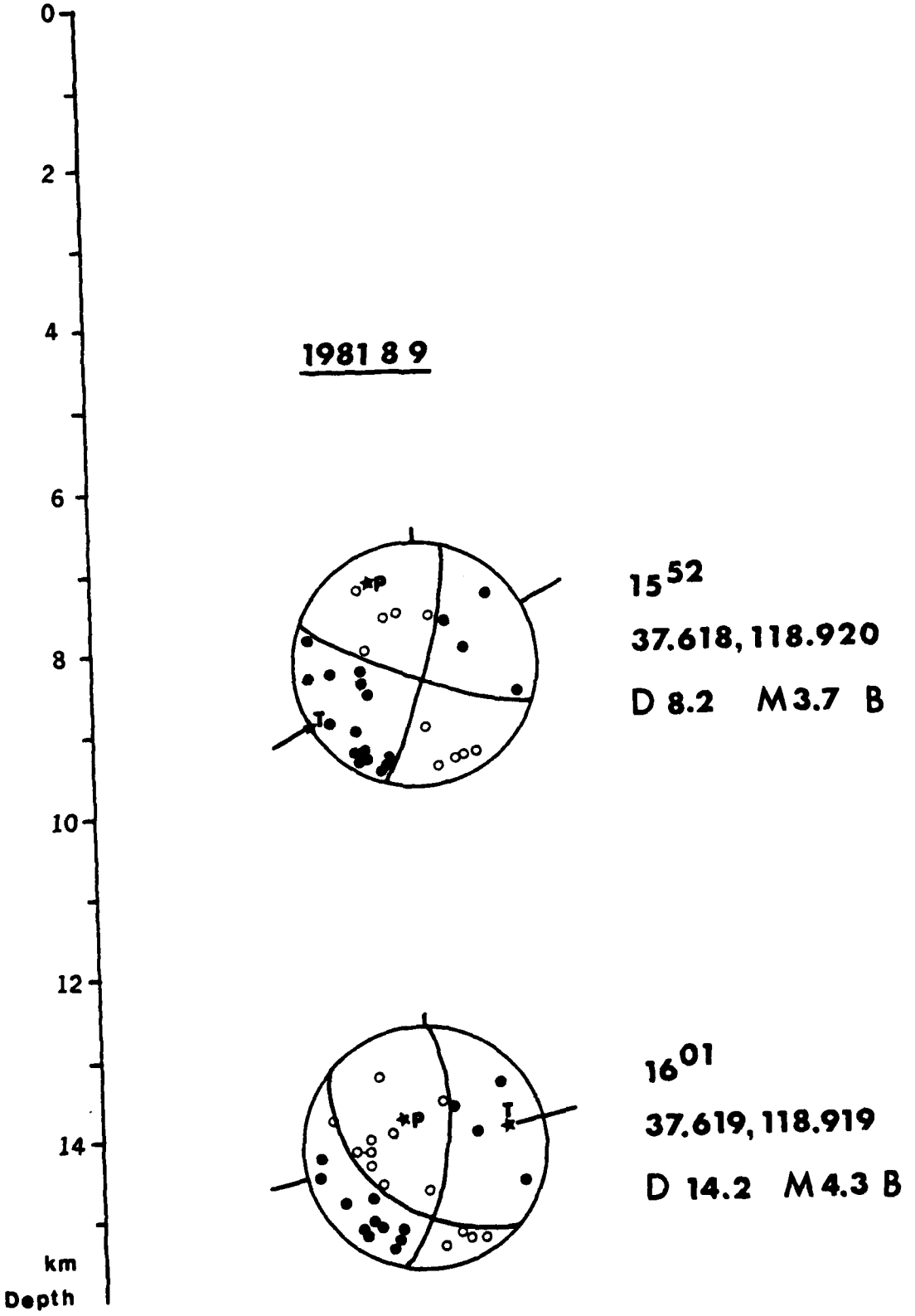
0
2
4
6
8
10
12
14
km
Depth
1981 8 9
P
T
P
I
15 52
37.618, 118.920
D 8.2 M3.7 B
16 01
37.619, 118.919
D 14.2 M4.3 B

Figure 5

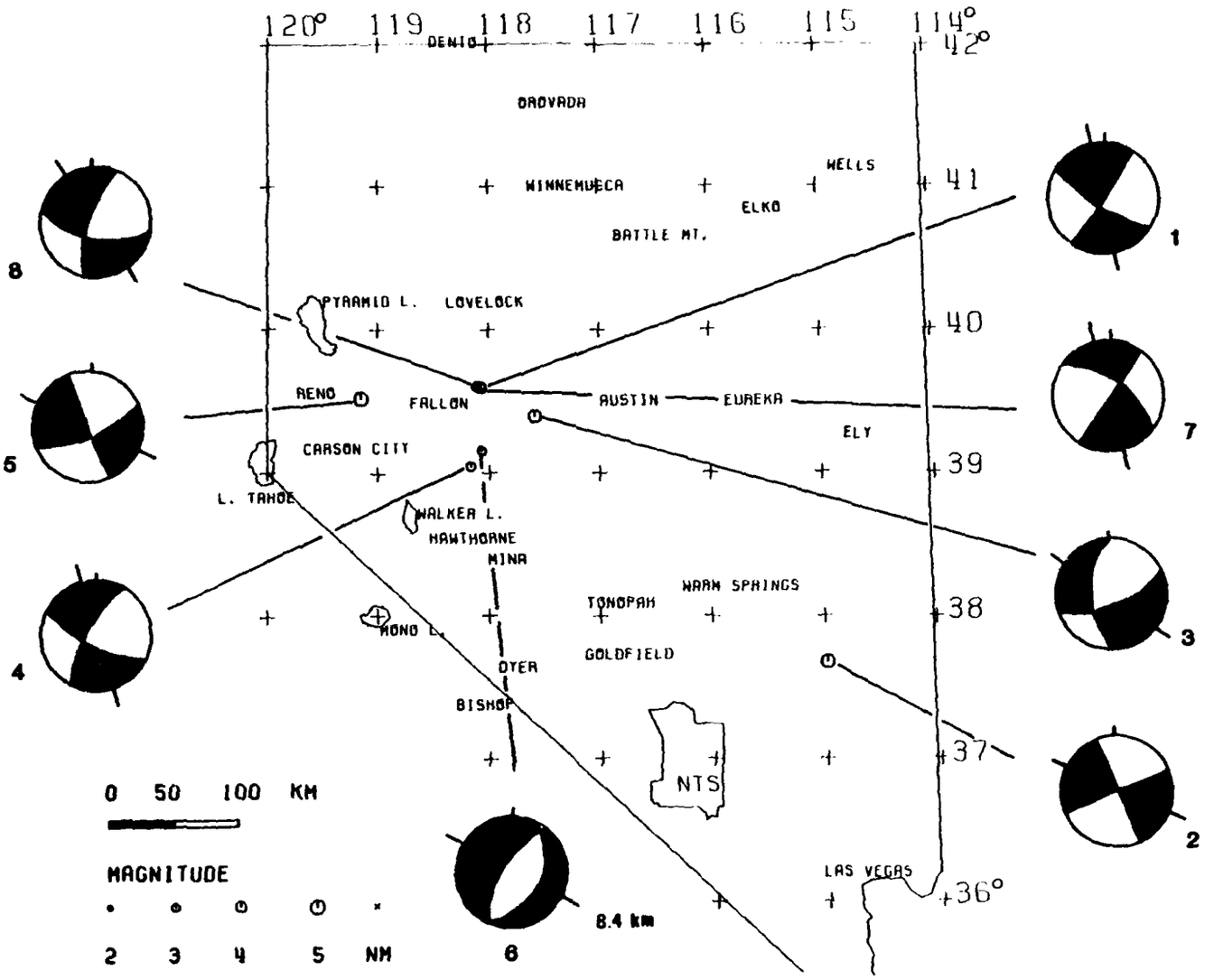
120°
119
118
117
116
115
114°
42°
41
40
39
38
37
36°
DENIO
ORDVADA
WINNEMUCCA
WELLS
ELKO
BATTLE MT.
PYRAMID L.
LOVELOCK
RENO
FALLON
AUSTIN
EUREKA
ELY
CARSON CITY
L. TAHOE
WALKER L.
HAWTHORNE
MINA
WARM SPRINGS
TONOPAH
MONO L.
GOLDFIELD
OTER
BISHOP
NTS
LAS VEGAS
0 50 100 KM
MAGNITUDE
2 3 4 5 NM
8.4 km
1
2
3
4
5
6
7
8

Figure 6

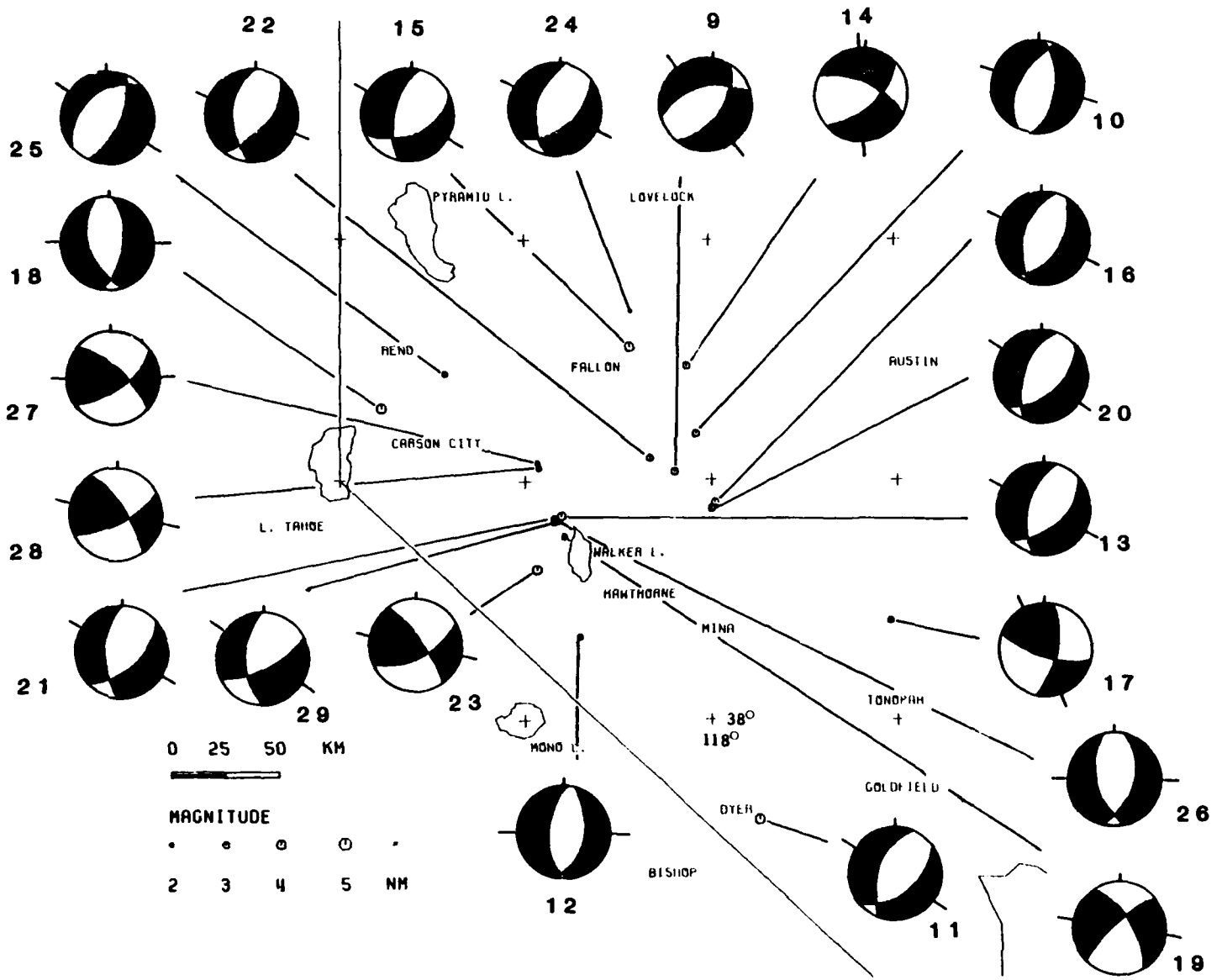
22
15
24
9
14
25
10
18
16
27
20
28
13
21
29
23
17
26
12
11
19
PYRAMID L.
LOVELOCK
RENO
FALLON
AUSTIN
CARSON CITY
L. TAHOE
WALKER L.
HAWTHORNE
MINA
TONOPAH
+ 38°
118°
MONO L.
GOLDFIELD
DYER
BISHOP
0 25 50 KM
MAGNITUDE
2 3 4 5 NM

Figure 7

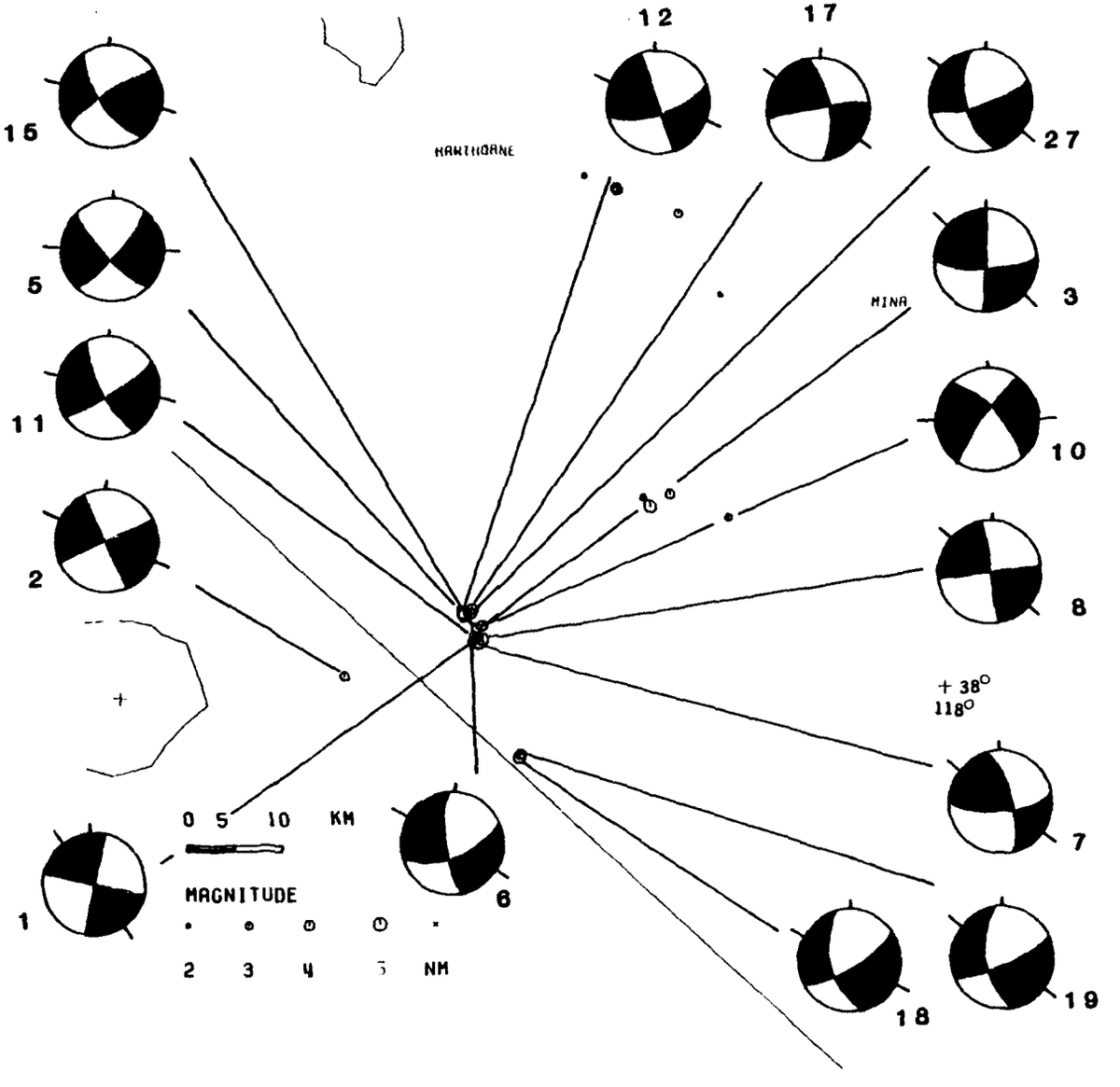
12
17
15
27
HAWTHORNE
5
MINA
3
11
10
2
8
+ 38°
118°
0 5 10 KM
7
MAGNITUDE
6
1
18
19
2 3 4 5 NM

Figure 8

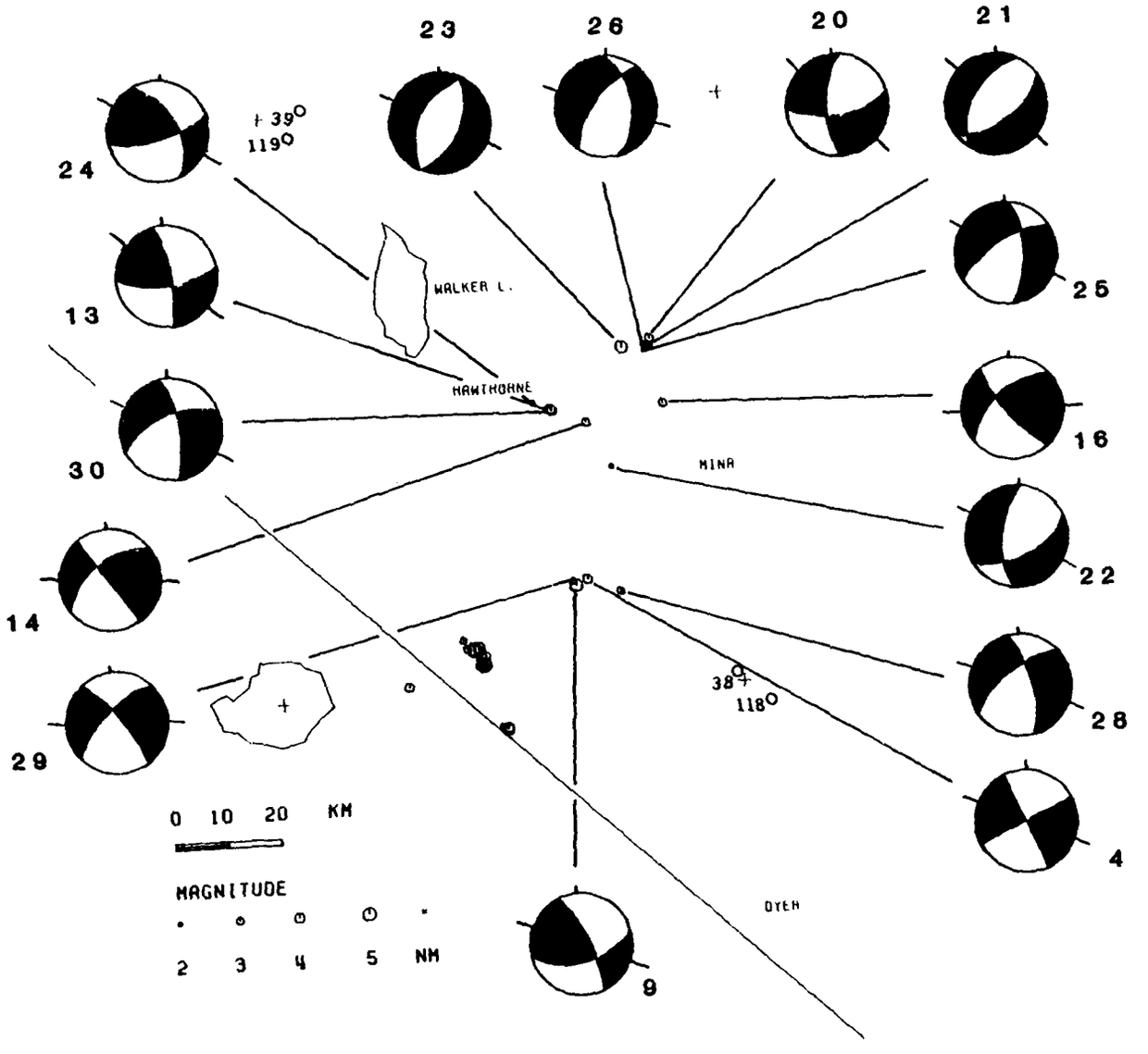
23
26
20
21
24
+ 39°
119°
WALKER L.
25
13
HAWTHORNE
16
30
MINA
22
14
38°
118°
28
29
0 10 20 KM
MAGNITUDE
2 3 4 5 NM
4
DYER
9

Figure 9

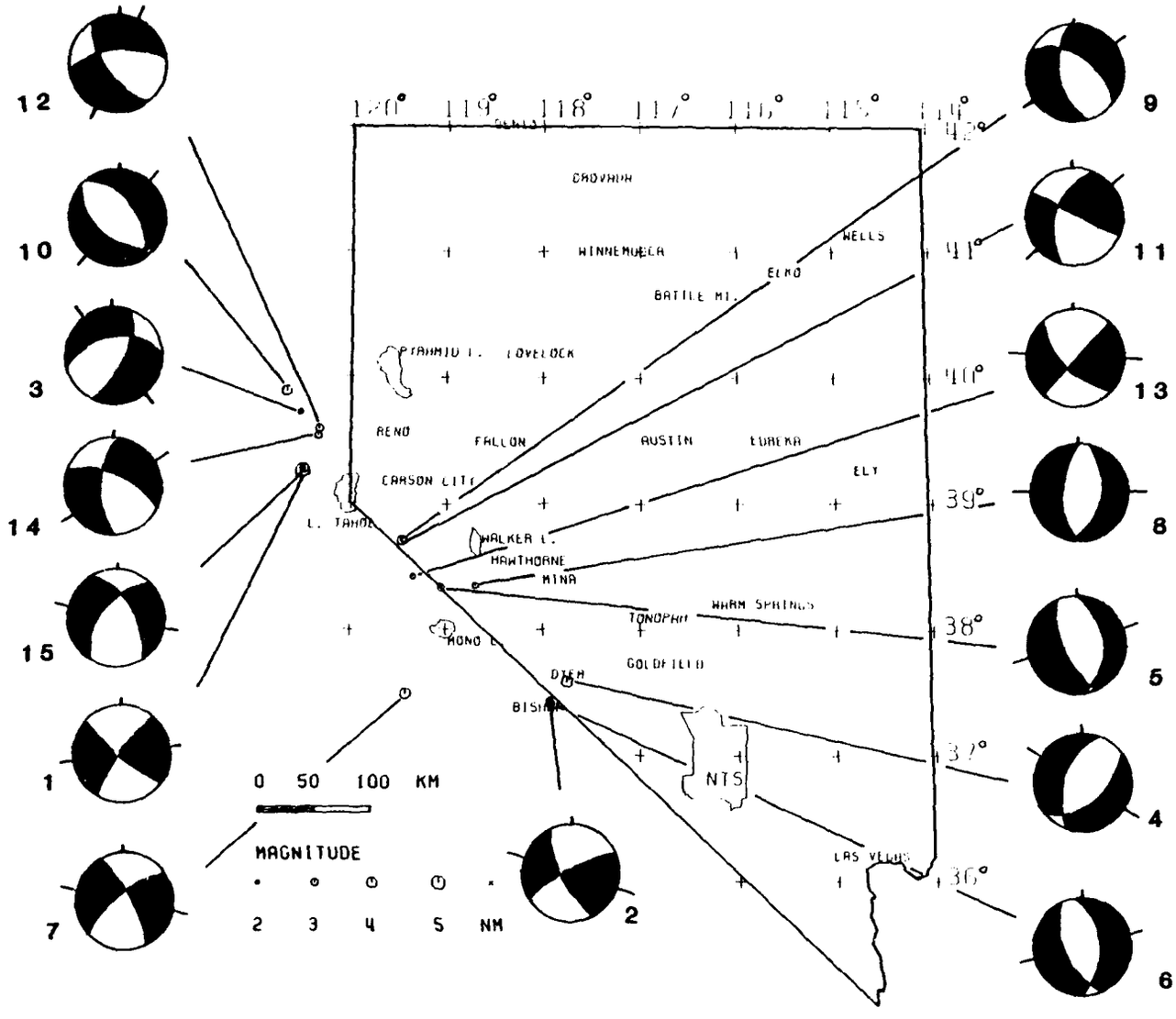
12
10
3
14
15
1
7
9
11
13
8
5
4
6
2
120°
119°
118°
117°
116°
115°
114°
42°
41°
40°
39°
38°
37°
36°
CROVADA
WINNEMUCCA
WELLS
ELKO
BATTLE MT.
PYRAMID L.
LOVELOCK
RENO
FALLON
AUSTIN
EUREKA
ELY
CARSON CITY
L. TAHOE
WALKER L.
HAWTHORNE
MINA
WARM SPRINGS
TONOPAH
MONO L.
GOLDFIELD
DYER
BISHOP
NTS
LAS VEGAS
0 50 100 KM
MAGNITUDE
2 3 4 5 NM

Figure 10

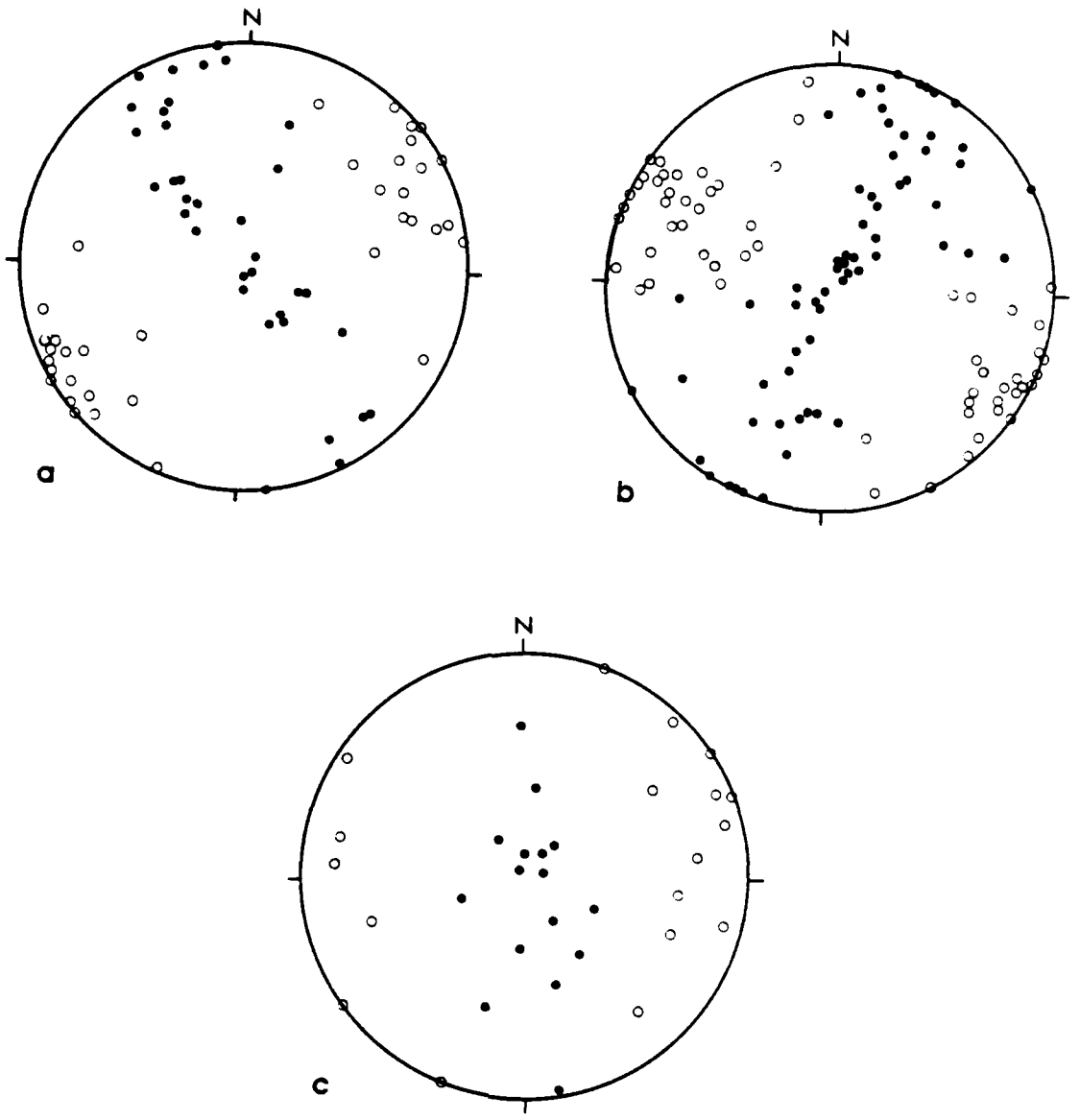

Figure 11

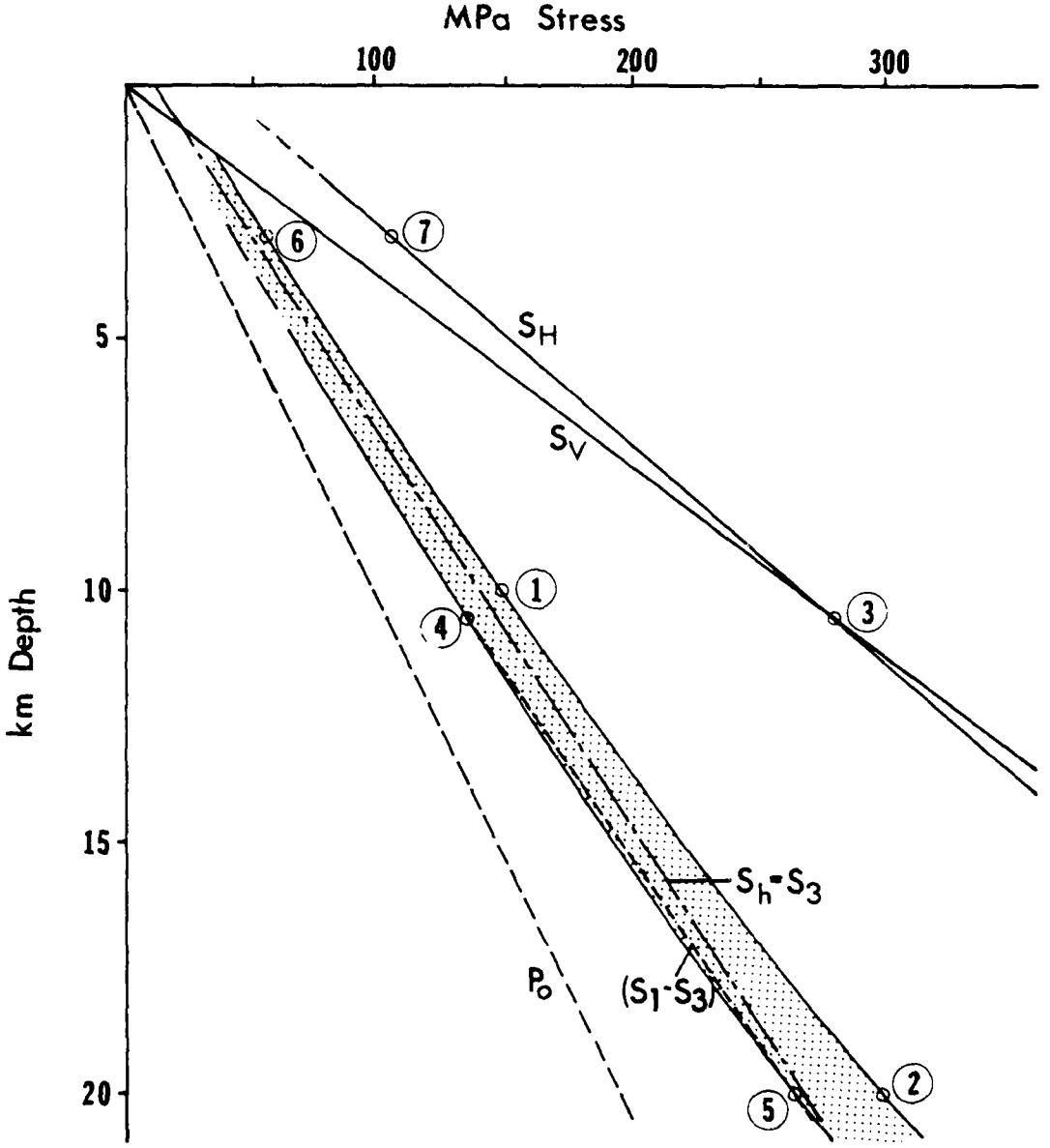
MPa Stress
100
200
300
km Depth
5
10
15
20
S_H
S_V
S_h
P_o
(S_1-S_3)
1
2
3
4
5
6
7

Figure 12

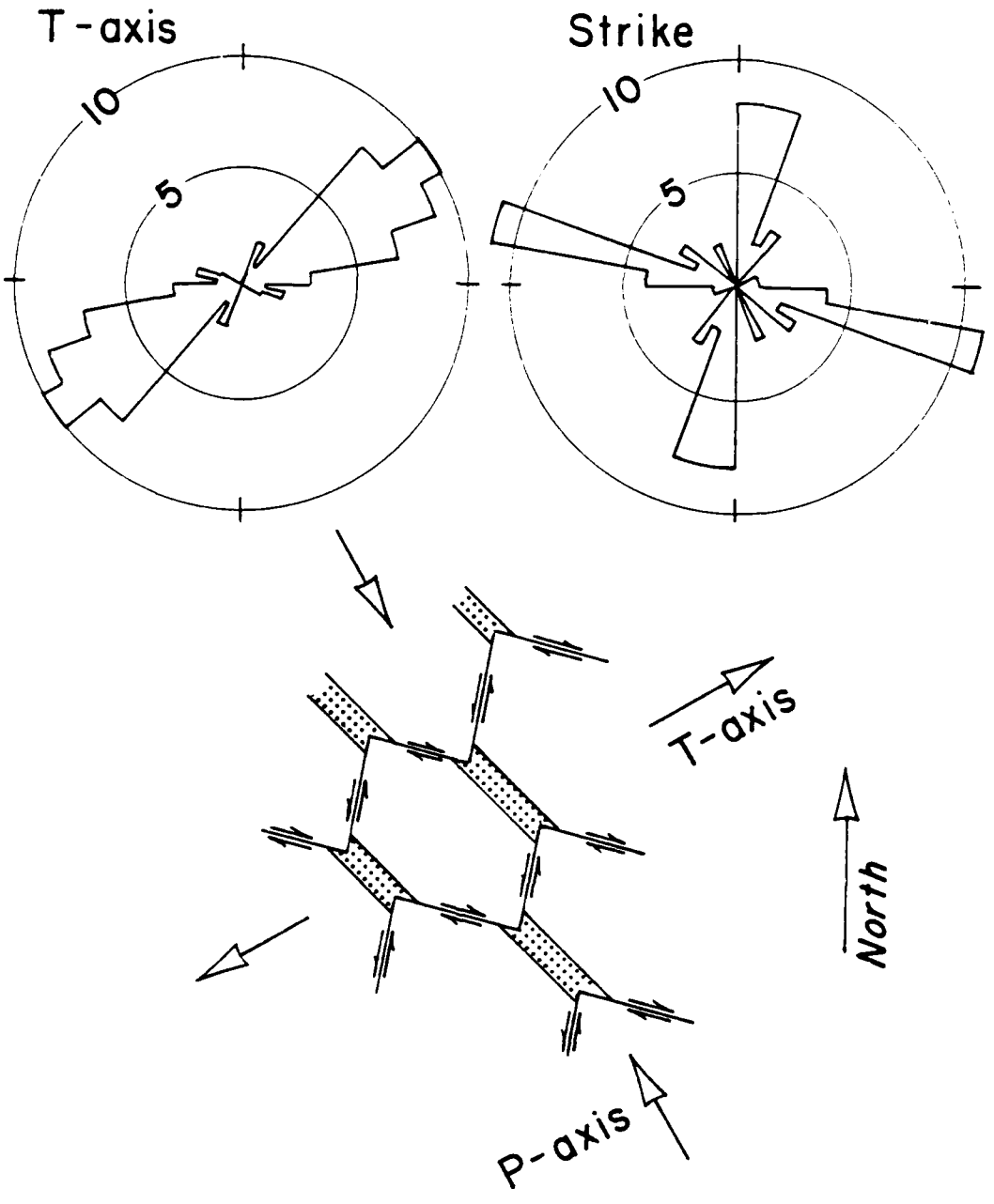

Figure 13


ATE
LME